
01 Apr 2022

Low-Intensity Blast Induces Acute Glutamatergic Hyperexcitability in Mouse Hippocampus Leading to Long-Term Learning Deficits and Altered Expression of Proteins Involved in Synaptic Plasticity and Serine Protease Inhibitors

Shanyan Chen


Heather R. Siedhoff

Hua Zhang

Pei Liu

et. al. For a complete list of authors, see https://scholarsmine.mst.edu/min_nuceng_facwork/1644

Follow this and additional works at: https://scholarsmine.mst.edu/min_nuceng_facwork

 Part of the [Explosives Engineering Commons](#), and the [Neuroscience and Neurobiology Commons](#)

Recommended Citation

S. Chen et al., "Low-Intensity Blast Induces Acute Glutamatergic Hyperexcitability in Mouse Hippocampus Leading to Long-Term Learning Deficits and Altered Expression of Proteins Involved in Synaptic Plasticity and Serine Protease Inhibitors," *Neurobiology of Disease*, vol. 165, article no. 105634, Elsevier, Apr 2022. The definitive version is available at <https://doi.org/10.1016/j.nbd.2022.105634>



This work is licensed under a [Creative Commons Attribution 4.0 License](#).

This Article - Journal is brought to you for free and open access by Scholars' Mine. It has been accepted for inclusion in Mining Engineering Faculty Research & Creative Works by an authorized administrator of Scholars' Mine. This work is protected by U. S. Copyright Law. Unauthorized use including reproduction for redistribution requires the permission of the copyright holder. For more information, please contact scholarsmine@mst.edu.



Low-intensity blast induces acute glutamatergic hyperexcitability in mouse hippocampus leading to long-term learning deficits and altered expression of proteins involved in synaptic plasticity and serine protease inhibitors

Shanyan Chen^{a,b,1}, Heather R. Siedhoff^{a,b,1}, Hua Zhang^{c,1}, Pei Liu^d, Ashley Balderrama^{a,b}, Runtong Li^{a,b}, Catherine Johnson^e, C. Michael Greenlief^d, Bastijn Koopmans^f, Timothy Hoffman^{a,c}, Ralph G. DePalma^{g,h}, De-Pei Li^c, Jiankun Cui^{a,b,*}, Zezong Gu^{a,b,*}

^a Truman VA Hospital Research Service, Columbia, MO 65201, USA

^b Department of Pathology & Anatomical Sciences, University of Missouri School of Medicine, Columbia, MO 65212, USA

^c Department of Medicine, University of Missouri School of Medicine, Columbia, MO 65212, USA

^d Charles W. Gehrke Proteomics Center, University of Missouri, Columbia, MO 65211, USA

^e Department of Mining and Nuclear Engineering, Missouri University of Science and Technology, Rolla, MO 65409, USA

^f Sylics (Synaptologics BV), Bilthoven, 3721, MA, the Netherlands

^g Office of Research and Development, Department of Veterans Affairs, Washington DC 20420, USA

^h Department of Surgery, Uniformed Services University of the Health Sciences, Bethesda, MD 20814, USA

ARTICLE INFO

Keywords:

Primary open-field blast
Glutamatergic hyperexcitability
Home-cage monitoring
Label-free proteomic quantitation
Chronic cognitive dysfunction

ABSTRACT

Neurocognitive consequences of blast-induced traumatic brain injury (bTBI) pose significant concerns for military service members and veterans with the majority of “invisible injury.” However, the underlying mechanism of such mild bTBI by low-intensity blast (LIB) exposure for long-term cognitive and mental deficits remains elusive. Our previous studies have shown that mice exposed to LIB result in nanoscale ultrastructural abnormalities in the absence of gross or apparent cellular damage in the brain. Here we tested the hypothesis that glutamatergic hyperexcitability may contribute to long-term learning deficits. Using brain slice electrophysiological recordings, we found an increase in averaged frequencies with a burst pattern of miniature excitatory postsynaptic currents (mEPSCs) in hippocampal CA3 neurons in LIB-exposed mice at 1- and 7-days post injury, which was blocked by a specific NMDA receptor antagonist AP5. In addition, cognitive function assessed at 3-months post LIB exposure by automated home-cage monitoring showed deficits in dynamic patterns of discrimination learning and cognitive flexibility in LIB-exposed mice. Collected hippocampal tissue was further processed for quantitative global-proteomic analysis. Advanced data-independent acquisition for quantitative tandem mass spectrometry analysis identified altered expression of proteins involved in synaptic plasticity and serine protease inhibitors in LIB-exposed mice. Some were correlated with the ability of discrimination learning and cognitive flexibility. These findings show that acute glutamatergic hyperexcitability in the hippocampus induced by LIB may contribute to long-term cognitive dysfunction and protein alterations. Studies using this military-relevant mouse model of mild bTBI provide valuable insights into developing a potential therapeutic strategy to ameliorate hyperexcitability-modulated LIB injuries.

1. Introduction

Blast-induced traumatic brain injury (bTBI) remains of great concern among military personnel and veterans. Approximately three-quarters

of combat casualties relate to blast exposure among soldiers serving in Iraq and Afghanistan from 2005 to 2009 (Belmont Jr et al., 2012). Traumatic Brain Injury Center of Excellence (TBI CoE), Defense Department recently reported that 82.3% of 444,328 military-related

* Corresponding authors at: Truman VA Hospital Research Service, Columbia, MO 65201, USA; Department of Pathology & Anatomical Sciences, University of Missouri-Columbia, School of Medicine, Columbia, MO 65212, USA

E-mail addresses: cuij@health.missouri.edu (J. Cui), Zezong.Gu@va.gov, guze@health.missouri.edu (Z. Gu).

¹ Indicates co-first authors.

<https://doi.org/10.1016/j.nbd.2022.105634>

Received 9 August 2021; Received in revised form 11 January 2022; Accepted 17 January 2022

Available online 22 January 2022

0969-9961/© 2022 The Authors.

Published by Elsevier Inc.

This is an open access article under the CC BY-NC-ND license

(<http://creativecommons.org/licenses/by-nc-nd/4.0/>).

TBI patients from 2000 to 2021 Q2 belong to mild TBI (TBICoE, 2021), known as signature “invisible injury,” characterizing these conflicts. Mild TBI caused by low-intensity blast (LIB) exposure during military occupational training also have been increasingly recognized, though assessing their neurological consequences remains a continuing challenge (Belding et al., 2021; DePalma and Hoffman, 2018; Simmons et al., 2020) in that LIB exposure do not result in loss or alterations of consciousness.

To investigate mild TBI induced by LIB exposure, we established an open-field LIB injury model simulating in combat and military training scenarios. The LIB exposure in mice was generated by detonation of 46.6 kPa peak overpressure approximating Army safety threshold level (Engel et al., 2019). With open-field blast, a nearly instantaneous rise in over pressure is followed by an exponential decay for both surface and suspended explosives (Rutter et al., 2021). Multiple focal ultrastructural abnormalities, alteration of proteomic profiles in the brain, and neuro-behavioral deficits have been found in the acute and subacute phases up to 1-month post blast injury without apparent pathological features of cell death and astrogliosis responses (Chen et al., 2018; Konan et al., 2019; Song et al., 2019; Song et al., 2018a; Song et al., 2018b; Song et al., 2018c). Compared with blunt impact from sport or automobile accidents with brain deformations related to lower strain rates and time frames in milliseconds, blast waves propagating at much higher strain rates of 10^2 – 10^3 /s (Panzer et al., 2012a; Panzer et al., 2012b) and time frames in microseconds (μ sec) or sub- μ sec cause distinctly different types of brain injury (Przekwas et al., 2016; Song et al., 2018a; Stuhmiller et al., 1991). Primary blast waves with high strain rates (Przekwas et al., 2016) and phonon decay in the brain (Kucherov et al., 2012; Song et al., 2018a; Song et al., 2018b) likely play essential roles in disturbing neural circuitry and damaging brain ultra-structures.

Glutamate, an essential excitatory neurotransmitter in the mammalian central nervous system (CNS), supports many physiological functions. Excessive release of glutamate may cause excitability-induced maladaptive neuroplasticity and neural injuries (Dorsett et al., 2017; Guerriero et al., 2015; Mattson, 2008). Moderate to severe TBIs are known to result in an excitatory-inhibitory imbalance in the neural circuit in rodents (Guerriero et al., 2015; Witkowski et al., 2019). Currently, whether LIB exposure results in synaptic dysregulation of posttraumatic glutamate release remains unexplored.

Cognition can be categorized into several distinct functions based on brain circuits and neuromodulators involved in this process (Pessoa, 2008). Cognition is achieved through sophisticated cellular and molecular mechanisms including synaptic plasticity (McIntosh, 2000), which plays an important role in learning and memory formation (Kennedy, 2013; Mayford et al., 2012). Cognitive flexibility refers to a learning skill that allows individuals to switch between different concepts or conditions to adjust behavior in novel, changing environments to facilitate the learning process. Progressive and accumulative clinical neuropsychiatric abnormalities may emerge in a period of months to years after blast exposure (Agoston, 2017; DePalma and Hoffman, 2018). The underestimation of long-term consequences of LIB exposure, particularly cognitive impairment, suggested a need to extend animal studies using novel, high-sensitivity quantitative approaches. We therefore evaluated the effect of open-field LIB exposure on glutamatergic synaptic inputs to hippocampal CA3 neurons, which are related to behavioral, functional and structural alterations associated with changes in synaptic plasticity after TBIs and mild cognitive impairment in early Alzheimer’s disease (Frautschy and Cole, 2010; Deuker et al., 2014; White et al., 2017; Witkowski et al., 2019). In addition, distinct cognitive functions on learning abilities and cognitive flexibility in the chronic phase at 3-months post-LIB exposure were assessed using an automated home-cage monitoring (HCM) system with minimal human interference and environmental stress. Moreover, quantitative proteomics and bioinformatic analysis were utilized to illustrate networks of hippocampal global-proteomes for molecular signaling effects on synaptic activity-related cognitive deterioration. This study showed that a single LIB

exposure induced hyperexcitation of hippocampal synapses followed by a long-term proteomic change accompanied by a long-term impairment of cognitive function. These findings provide a platform to examine therapeutic strategies to prevent or mitigate long-term cognitive learning disorders related to acute glutamatergic hyperexcitability.

2. Materials and methods

2.1. Open-field primary blast injury in mice

All animal experiments were performed in a blinded manner and in accordance with the University of Missouri approved protocols for the Care and Use of Laboratory Animals and the Animal Research: Reporting of In Vivo Experiments (ARRIVE) guidelines. 74 male C57BL/6J mice (The Jackson Laboratory, Bar Harbor, ME) aged 2 months old were housed with a 12-h light/dark cycle in home-cages containing bedding, with ad libitum access to food and water. Presence of female gonadal hormones may have profound effects on pathophysiological and behavioral outcomes following TBI, such as mortality, edema, cell death, neuroinflammation, sensorimotor function, cognitive function, and anxiety/depression-like behaviors (Rubin and Lipton, 2019; Wagner et al., 2004). As the first time accessing long-term effects of open-field LIB exposure with multi-faceted approaches, only adult male mice were used in this study. Open-field LIB exposure were conducted at the Missouri University of Science & Technology as previously reported (Chen et al., 2018; Konan et al., 2019; Song et al., 2019; Song et al., 2018a; Song et al., 2018b; Song et al., 2018c). Animals were assigned randomly into two groups, which were double-blinded to investigators analyzing experimental outcomes: LIB-exposed mice and sham controls. Animals were anesthetized using intraperitoneal injection of 10 μ L/g body weight of ketamine/xylazine mixture (12.5 mg/mL ketamine and 0.675 mg/mL xylazine). The elimination half-life of ketamine is approximately 13 min when administered intraperitoneally (Jaber et al., 2014; Maxwell et al., 2006). Mice in sham control group underwent the identical anesthesia procedures only without LIB exposure. Mice were placed in metal mesh animal holders in prone position on the platforms at 3-m distance away from detonation of a 350 g C4 explosion generating a magnitude of 46.6 kPa peak overpressure, a maximal impulse of 60 kPa*ms, and in the absence of head or bodily motion, as described previously (Konan et al., 2019; Rutter et al., 2021; Song et al., 2019; Song et al., 2018c). Following blast wave exposure, animals were removed from the platform and returned to their original cages. After recovery from anesthesia, mice were monitored for at least 15–30 min and allowed access to food and water ad libitum.

2.2. Brain slice preparation and electrophysiological recordings

Sixteen male C57BL/6J mice were sacrificed at 1-, 7-days and 3-months post LIB exposure for the electrophysiological recordings ($n = 4$ in sham controls, $n = 4$ in mice at 1-, 7-days and 3-months post LIB exposure accordingly). Preparation of the brain slices for electrophysiological recordings was referred as previously described (Li et al., 2017; Zhou et al., 2018). Briefly, the mice were decapitated under anesthesia with 2–3% isoflurane and the brain quickly removed and put into an ice-cold cutting solution containing (in mM) 2.5 KCl, 1.2 NaH_2PO_4 , 30 NaHCO_3 , 25 Glucose, 20 HEPES, 93 NMDG, 0.5 CaCl_2 , 10 MgCl_2 and saturated with 95% O_2 and 5% CO_2 . Coronal slices (400 μ m thick) containing the hippocampus were sectioned using a vibrating microtome (VT1200 S; Leica Biosystems Inc. Buffalo Grove, IL, USA). The brain slices were incubated in the cutting solution at 37 °C for 10 mins and transferred into an artificial cerebral spinal fluid (aCSF) as for patch-clamp recording containing (in mM) 126 NaCl, 3 KCl, 1.5 MgCl_2 , 2.4 CaCl_2 , 1.2 NaH_2PO_4 , 10 glucose and 26 NaHCO_3 saturated with 95% O_2 and 5% CO_2 at 37 °C for at least 1 h before recording.

The hippocampal slices were continuously perfused with aCSF saturated by 95% O_2 and 5% CO_2 (3.0 mL/min) at 34 °C maintained by

an inline solution heater. The neurons in CA3 area were visualized under an upright microscope. The mEPSCs were recorded using whole-cell patch-clamp (Axon 700B amplifier and DigiData 1550B, Molecular Device) in the presence of tetrodotoxin (TTX, 1 μ M) and GABA_A receptor antagonist bicuculline (20 μ M) at a holding potential of -60 mV. DNQX (20 μ M) was used to block signals from non-NMDA receptors. The recording glass pipette (4–8 M Ω) was filled with an internal solution containing (in mM) 135.0 potassium gluconate, 5.0 tetraethylammonium, 2.0 MgCl₂, 0.5 CaCl₂, 5.0 HEPES, 5.0 EGTA, 5.0 Mg-ATP and 0.5 Na-GTP (adjusted to pH 7.2–7.4 with KOH; 290–300 mM). A sodium channel blocker, lidocaine N-ethyl bromide (10.0 mM), was included in the pipette solution to block the firing activity of the recorded neuron. The mEPSCs were recorded with continuing TTX perfusion, when the mEPSCs were stable approximately 10 min after starting TTX perfusion. The input resistance was monitored and rather stable during the recording period. We did not include the recording of the neurons for data analysis if input resistance was significantly altered (> 15%). Agents including TTX, bicuculline, and NMDA receptor antagonist AP5 at the final concentration (50 μ M) were administered into the aCSF solution through a syringe pump (Ma et al., 2018).

2.3. Automated assessments of learning ability in a home-cage environment

Learning ability evaluation in 58 male C57BL/6J mice ($n = 24$ in sham controls and $n = 34$ in LIB-exposed mice) was assessed at 3-months post LIB exposure with the PhenoTyper[®] home-cages (Model 3000, Noldus Information Technology, The Netherlands) and CognitionWall[™] system (Noldus Information Technology, The Netherlands) as previously described (Kovacevic et al., 2018; Logan et al., 2019; Rummelink et al., 2016a; Rummelink et al., 2016b). All mice were familiar with the home-cage environment by being placed in the PhenoTyper for three days before conducting the CognitionWall assessments. The PhenoTyper protocols were obtained from Sylics and data were analyzed using AHCODA (Sylics, Bilthoven, The Netherlands). At 3:00 pm, regular food chows were removed. At 3:45 pm CognitionWall devices were inserted into the PhenoTyper at the back-left corner with the dispensers containing food pellets (Dustless Precision Pellets[®], 20 mg, Rodent Grain-Based Diet, Bio-Serv, New Jersey). The CognitionWall has three entrances (*left*, *middle*, and *right*) placed in front of the food dispenser. Mice were required to enter the CognitionWall through the *left* entrance in order to receive a reward of one food pellet every fifth time of the correct entry, named as a Fixed Ratio 5 schedule (FR5 schedule) during the initial discrimination phase. Mice behavior was automatically recorded through a 24/7, infrared-sensitive video-based observation system located on the top unit of the PhenoTyper. Mice were continuously monitored for 48 h of initial discrimination learning. After 48 h of initial discrimination learning, the CognitionWall protocol switched automatically and the correct entrance was changed to the *right* entrance following the same FR5 schedule, which requires the animal to extinguish the previous learning and acquire a new response, as for assessing the reversal learning ability for cognitive learning flexibility. All the animal tracking data were acquired through the EthoVision XT software v14 (Noldus Information Technology, The Netherlands) and sampled at a rate of 15 fps. Data were uploaded to the web-based AHCODA-DB (Sylics, Bilthoven, The Netherlands) for meta-analysis (Supplemental Figs. 2 and 3).

2.4. Protein digestion for tandem mass spectrometry (MS/MS) analysis

Ten male C57BL/6J mice ($n = 5$ in sham controls and $n = 5$ in LIB-exposed mice) were sacrificed at 3-months post LIB exposure, after the CognitionWall assessments, for the label-free proteomic quantitation by tandem mass spectrometry (MS/MS) analysis. Cerebral hippocampus was dissected and processed as described previously (Song et al., 2019). Briefly, lyse sample buffer (2% sodium dodecyl sulphate [SDS], 0.5 M

tetraethylammonium bicarbonate [TEAB], pH 8.5), protease inhibitor cocktail was added to each brain tissue specimen. Specimens were homogenized by Glas-Col stringer 099C K43 (Glas-Col LLC, IN) and centrifuged at $17,000 \times g$ for 20 min at 4 °C. Supernatant was collected and then precipitated by acetone. Four volumes of cold acetone were added to the protein samples and incubated at -20 °C overnight. The protein pellets were recovered by centrifugation at $16,100 \times g$ for 10 min at 4 °C and washed by 80% acetone twice. The final protein pellets were suspended in 6 M urea, 2 M thiourea and 100 mM ammonium bicarbonate. The protein concentration was determined using Pierce 660nm Protein Assay (Thermo Fisher Scientific) according to the manufacturer's protocol. Fifty μ g proteins from each sample were reduced by 10 mM dithiothreitol (DTT) at RT for 1 h. and alkylated by 40 mM iodoacetamide (IAA) at RT for 1 h in the dark. The excess of IAA was quenched by adding 40 mM DTT and incubated for 30 min. Before trypsin digestion, Lys-C (mass spectrometry grade, Promega) was added to each sample at a 1:70 enzyme-to-protein mass-ratio and incubated at 37 °C for 3 h. Then the urea buffer was diluted to less than 1 M urea by Milli-Q water. Trypsin (Promega) was added at a 1:50 enzyme-to-protein mass-ratio and were incubated at 37 °C overnight. The digested peptides were purified by Pierce C18 Tips according to the manufacturer's protocol (Thermo Fisher Scientific).

2.5. Spectra library generation

To generate a comprehensive spectra library, twenty μ g of purified peptides from each sample were combined and fractionated using a high pH reversed-phase peptide fractionation kit according to the manufacturer's protocol (Thermo Fisher Scientific). In total 8 fractions were collected, lyophilized and resuspended in 5% acetonitrile, 0.1% formic acid. The resuspended peptides were analyzed using Bruker timsTOF Pro mass spectrometer attached to a nanoElute LC (Bruker) system. The samples were loaded onto a trap column of 300 μ m i.d. x 5 mm with C8 PepMap100 100 Å, 5 μ m (Thermo Fisher Scientific). Then the peptides were separated by an in-house packed analytical column of 75 μ m i.d. x 20 cm with BEH C18, 130Å, 1.7 μ m (Waters, USA). The peptides were eluted at a flow rate of 300 nL/min with 90 min LC gradient: initial condition was 2% B (A: 0.1% formic acid in water, B: 99.9% acetonitrile, 0.1% formic acid), followed by 20 min ramp to 17% B, 17–25% B over 33 min, 25–37% B over 16 min, gradient of 37% B to 80% B over 7 min, hold at 80% B for 9 min, ramp back to 2% B in 1 min and hold at initial conditions for 4 min. The timsTOF Pro was operated in the data-dependent acquisition (DDA)-parallel accumulation serial fragmentation (PASEF) mode. Duty cycle was locked to 100%. Ion mobility coefficient ($1/K_0$) value was set from 0.6 to 1.6 Vs \cdot cm⁻². MS data were collected over m/z range of 100 to 1700. During MS/MS data collection, each tims cycle contained one MS and ten PASEF MS/MS scan. Exclusion was active after 0.4 min.

2.6. Data-independent acquisition and bioinformatic analysis

Data-independent acquisition (DIA) data were acquired using a timsTOF Pro operated in DIA-PASEF mode (Meier et al., 2020). MS data were collected over an m/z range of 400 to 1200 and an ion mobility range of 0.57 to 1.47 Vs \cdot cm⁻². Duty cycle was locked to 100%. A total of 64 DIA-PASEF windows were used (25 Th isolation windows) (Meier et al., 2020). The DIA-PASEF data were analyzed according to the reference of Vadim Demichev et al. (Demichev et al., 2021). Briefly, the spectral library was generated in FragPipe platform (v.15) with MSFragger (Kong et al., 2017; Yu et al., 2020) (v.3.2), Philosopher (da Veiga Leprevost et al., 2020) (v.3.4.13), and EasyPQP (v.0.1.11). Uniport Mouse (UP00000589) reviewed protein database with common contaminant proteins (total 17,174 sequences) was used. Data were searched with the following parameters: trypsin digestion with two missed cleavage allowed; precursor and fragment mass error 20 ppm; mass calibration and parameter optimization enabled; isotope error of

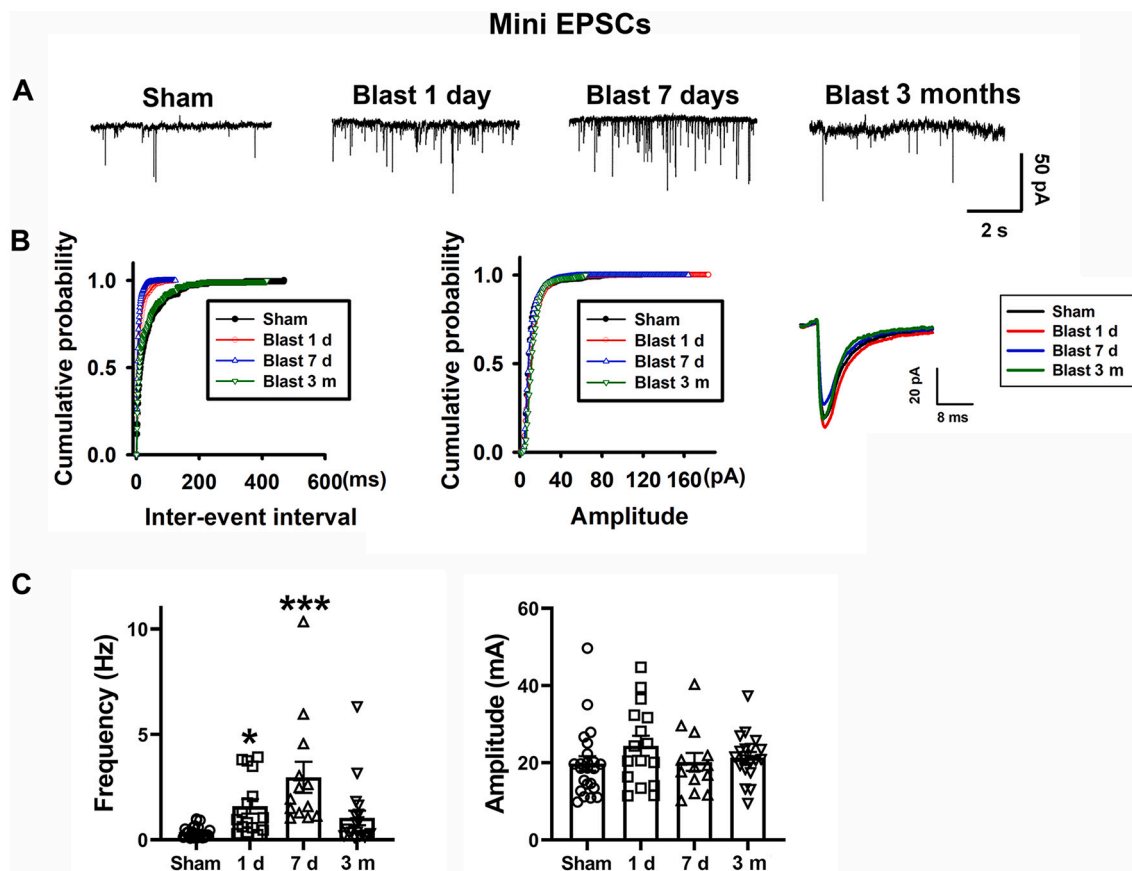


Fig. 1. LIB injury enhanced glutamatergic synaptic inputs to hippocampal CA3 neurons.

Representative traces showing mEPSCs recorded from sham controls and LIB-exposed mice at different time points post injury (A). Cumulative probability plots and average traces of mEPSCs (B) and summary data of the frequency and amplitude of mEPSCs (C) depicting that compared with sham control mice. The frequencies of mEPSC significantly increased at 1- and 7-days post injury and returned to similar levels in sham controls at 3-months post injury. The amplitudes did not change significantly between two groups (C). * $p < 0.05$, *** $p < 0.001$ compared with sham controls.

0/1/2; peptide length 7–50; cysteine carbamidomethylation as a fixed modification; methionine oxidation and acetylation at protein N-terminus as variable modifications; A minimum of 15 fragment peaks and the top 300 peaks used as initial spectral processing settings. PeptideProphet and ProteinProphet were used to filter to 1% protein-level false-discovery rate (FDR) using the picked FDR strategy. Finally, EasyPQP was used to generate the spectra library which was filtered to 1% protein and 1% peptide-level FDR. DIA-NN (v.1.7.15) was used to search the DIA-PASEF data with the generated spectra library from MSFragger. The MS1 and MS2 mass accuracy were set to 10 ppm. Match-between-runs (MBR) was enabled. All other settings were left default. The result was filtered at 1% precursor FDR, precursor q -value $< 1\%$, global protein q -value $< 1\%$ and intensity of 1000.

Proteins identified in at least three samples per group were included for further quantitation and bioinformatic analysis. Each protein's intensity was normalized to the total intensity. Protein-protein interaction analysis was conducted using the STRING database (Szklarczyk et al., 2019) and visualized in Cytoscape software (v3.8.2) (Shannon et al., 2003). The graphs were generated in R platform.

2.7. Statistical analyses

All experiments were performed in a randomized-blinded manner. Electrophysiological dataset was analyzed using Prism software (GraphPad Software, La Jolla, CA). Data are presented as mean values \pm SEM. One-way ANOVA or Repeated measures ANOVA followed by the Dunnett's and Tukey's post hoc tests was used for any comparisons of more than two groups. Kruskal-Wallis test was used to compare data

with skewed distribution. $p < 0.05$ was considered statistically significant. Behavioral analysis was accessed with Prism software (GraphPad Software, La Jolla, CA). Data are expressed as mean values \pm SEM and were analyzed by unpaired one-tailed Student's t -test for any two-group comparisons based on predictions formulated with prior data. Entries to criterion were analyzed by two-way repeated-measures ANOVA and Bonferroni multiple comparisons. Survival curves of group differences were assessed using the Log-rank (Mantel-Cox) test for differences between two Kaplan-Meier survival curves. Pearson correlation analysis was used to determine the correlations between different analysis in a one-tailed test. For statistical analysis of proteomic datasets, unpaired two-tailed Student t -test was performed among sham and blast group. Proteins with a p -value less than 0.05 and fold change larger than 1.3 and intensity at least 3000 was considered as a significant change.

3. Results

3.1. Exposure to LIB enhanced glutamatergic synaptic inputs to hippocampal CA3 neurons

Hippocampus is vulnerable to blast injury (Engel et al., 2019). Here we first extended our previous research from identifying LIB-induced ultrastructural abnormalities to evaluating synaptic function in mouse hippocampus (Konan et al., 2019). To examine effects of LIB exposure on synaptic function, we first measured glutamatergic synaptic inputs to hippocampal CA3 neurons through assessing miniature excitatory postsynaptic currents (mEPSCs) in brain slice preparations. The frequency and amplitude of mEPSCs were analyzed from LIB-exposed mice

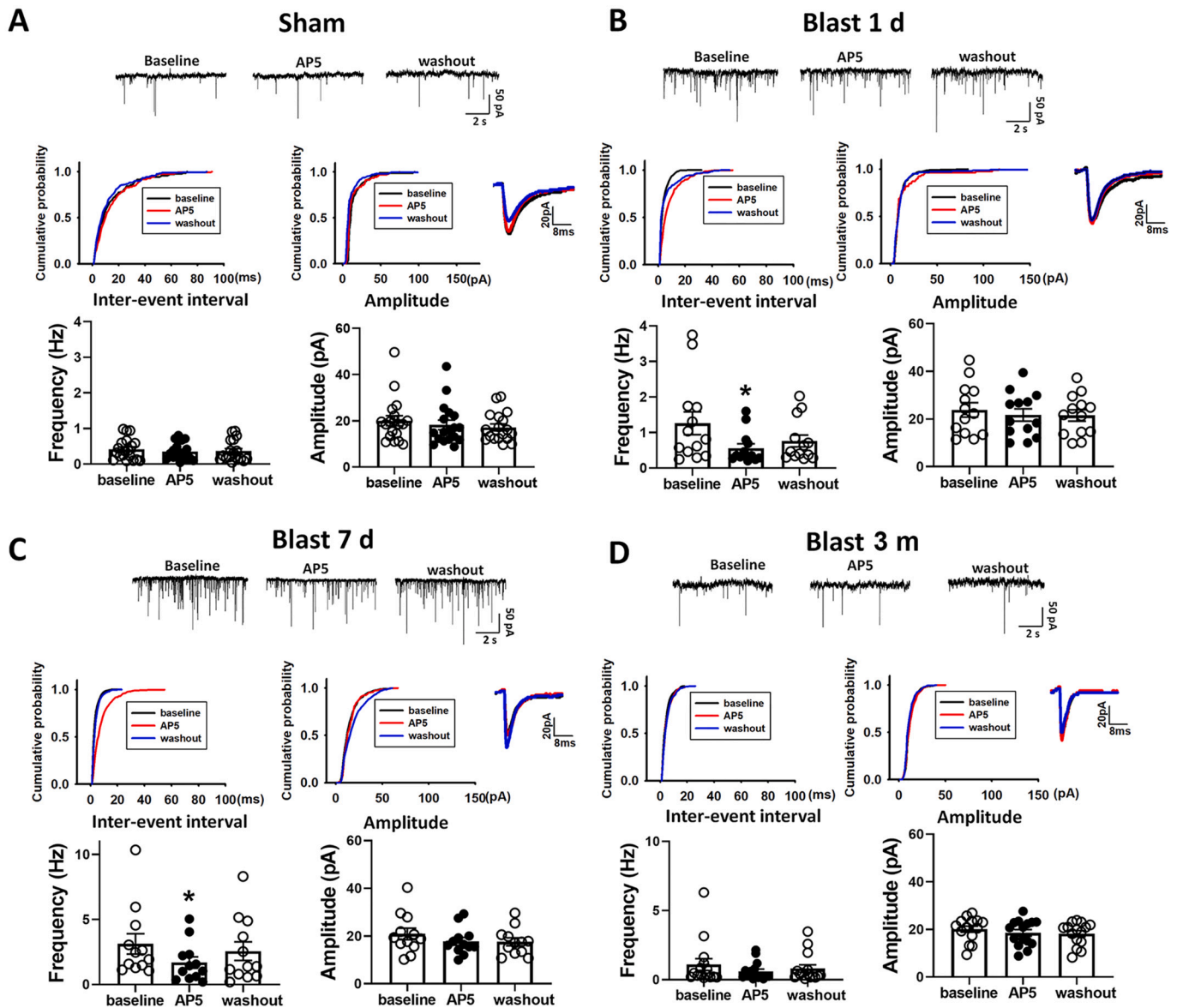


Fig. 2. Role of NMDA receptors in the effect of LIB exposure on mEPSCs.

Representative traces, cumulative plots, and summary data of averaged frequency and amplitude of mEPSCs showed the effect of bath application of 50 μ M AP5 on mEPSCs recorded from CA3 neurons in brain slices from sham controls (A), 1-day post injury (B), 7-days post injury (C) and 3-months post injury (D). * $p < 0.05$ compared with baseline values within the group.

and sham controls at different time points at 1-, 7-days and 3-months post LIB exposure (Fig. 1A). Cumulative probability analysis of mEPSCs revealed that the distribution patterns of the inter-event interval of mEPSCs recorded in CA3 neurons from LIB-exposed mice at 1- and 7-days post injury were shifted to the left compared with that in sham controls (Fig. 1B). The averaged frequencies of mEPSCs recorded in CA3 neurons from LIB-exposed mice at 1- and 7-days post injury were significantly higher than those in sham controls. The frequencies of mEPSCs did not differ between LIB-exposed mice and sham controls at 3-months post injury (sham: $n = 22$ neurons from 4 mice; 1-day post LIB: $n = 16$ neurons from 4 mice, $p = 0.029$; 7-days post LIB: $n = 13$ neurons from 4 mice, $p = 0.0001$; 3-months post LIB: $n = 19$ neurons from 4 mice, $p = 0.5734$, Kruskal-Wallis test, H-value = 29.25 for Fig. 1C). The amplitudes of mEPSCs did not differ significantly between LIB-exposed mice and sham controls (Fig. 1C). Application of 20 μ M 6,7-dinitroquinoxaline-2,3-dione (DNQX), a selective non-NMDA receptor antagonist, abolished mEPSCs recorded in CA3 neurons in both LIB-exposed mice and sham controls (Supplemental Fig. 1).

To determine the role of *N*-methyl-D-aspartate receptors (NMDARs) in the increased frequency of mEPSCs in LIB-exposed mice, bath application of AP5 (50 μ M), a specific NMDAR antagonist, significantly decreased the frequencies of mEPSCs in CA3 neurons from LIB-exposed mice at 1- and 7-days post injury. AP5 application did not change the frequencies of mEPSCs recorded in CA3 neurons from LIB-exposed mice at 3-months post injury (sham: $n = 18$ neurons from 4 mice, $p = 0.1062$, $F_{(1.755, 29.83)} = 2.488$; 1-day post LIB: $n = 13$ neurons from 4 mice, $p = 0.0269$, $F_{(1.155, 13.86)} = 5.795$; 7-days post LIB: $n = 12$ neurons from 4 mice, $p = 0.037$, $F_{(1.556, 17.11)} = 4.378$; 3-months post LIB: $n = 15$ neurons from 4 mice, $p = 0.1256$, $F_{(1.115, 15.61)} = 2.587$. Repeated measures ANOVA for Fig. 2). Bath application of AP5 did not alter the amplitudes of mEPSCs in LIB-exposed mice and sham controls (Fig. 2). These findings suggest that NMDARs importantly modulate glutamatergic synaptic inputs in the hippocampus of LIB-exposed mice.

We also found that LIB induced a burst pattern of glutamatergic mEPSCs recorded in CA3 neurons from LIB-exposed mice (Fig. 3A). The numbers of bursts mEPSCs recorded in CA3 neurons from LIB-exposed

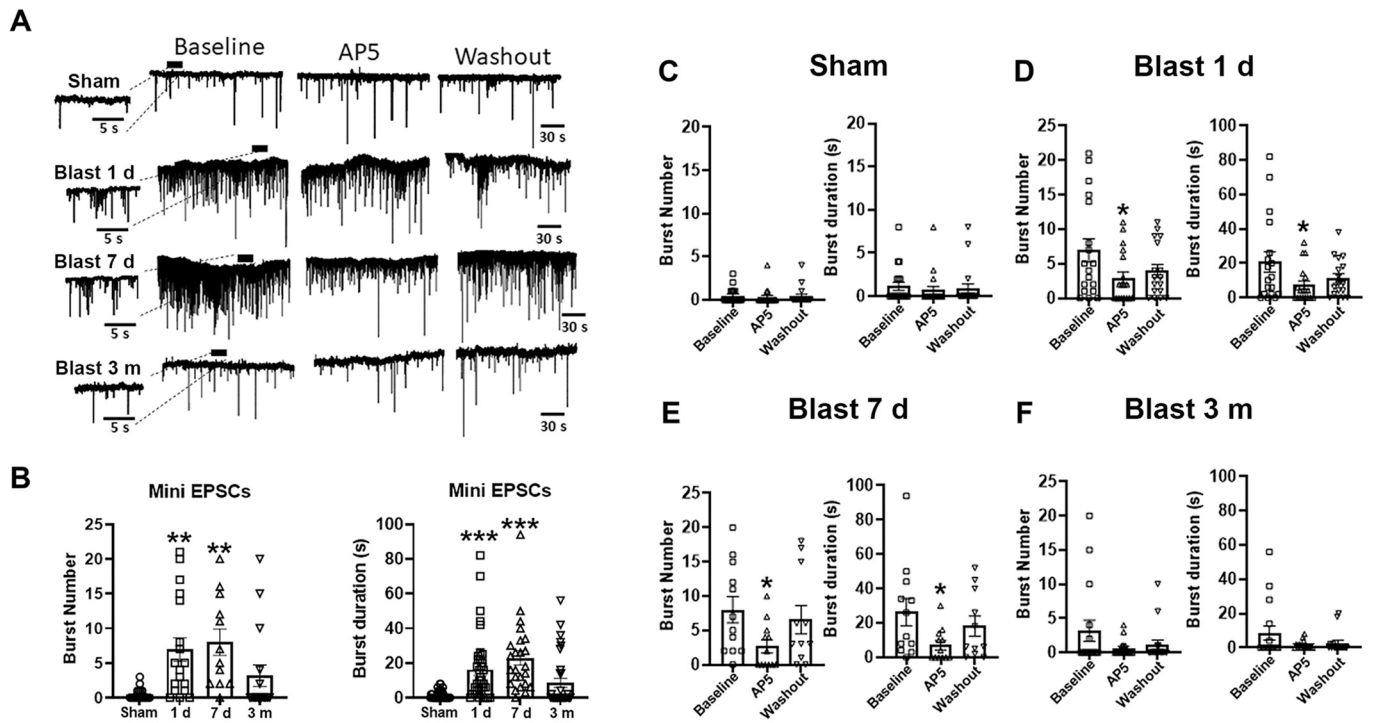


Fig. 3. LIB induced a burst pattern in glutamatergic synaptic inputs to hippocampal CA3 neurons.

Raw tracings depicting the effect of AP5 on mEPSCs recorded from sham controls and LIB-exposed mice at different time points post injury (A). Summary data showing that LIB exposure significantly increased the numbers of burst mEPSCs and the burst duration at 1- and 7-days post injury (B). Summary data showing the effect of AP5 on the numbers and duration of burst mEPSCs in sham controls and LIB-exposed mice at different time points post injury (C–F). * $p < 0.05$, compared with baseline values within each group. ** $p < 0.01$ and *** $p < 0.001$ compared with values in sham group.

mice at 1- and 7-days post injury were significantly higher than that in sham controls. The numbers of bursts at 3-months post injury did not differ significantly between LIB-exposed mice and sham controls (sham: $n = 19$ neurons from 4 mice; 1-day post LIB: $n = 18$ neurons from 4 mice, $p = 0.0051$; 7-days post LIB: $n = 12$ neurons from 4 mice, $p = 0.0034$; 3-months post LIB: $n = 16$ neurons from 4 mice, $p = 0.4966$, $F_{(3, 61)} = 6.113$. One-way ANOVA for Fig. 3B). The duration of burst mEPSCs was also significantly longer in LIB-exposed mice at 1- and 7-days, but not at 3-months post injury compared to sham controls (1-day post LIB: $p = 0.0005$; 7-days post LIB: $p = 0.0001$; 3-months post LIB: $p = 0.2374$, $F_{(3, 126)} = 10.99$. One-way ANOVA for Fig. 3B). Bath application of AP5 (50 μM) significantly decreased the burst numbers (1-day post LIB: $n = 17$ neurons from 4 mice, $p = 0.0157$, $F_{(1,460, 23.36)} = 5.712$; 7-days post LIB: $n = 11$ neurons from 4 mice, $p = 0.0042$, $F_{(1,835, 18.35)} = 7.798$) and duration (1-day post LIB: $p = 0.0302$, $F_{(1,267, 20.28)} = 4.956$; 7-days post LIB: $p = 0.013$, $F_{(1,386, 13.86)} = 7.023$. Repeated measures ANOVA) of mEPSCs in CA3 neurons from LIB-exposed mice at 1- and 7-days post injury (Fig. 3D and E). AP5 application did not significantly alter the burst numbers (sham: $n = 18$ neurons from 4 mice, $p = 0.4976$, $F_{(1,828, 31.07)} = 0.6879$; 3-months post LIB: $n = 16$ neurons from 4 mice, $p = 0.0848$, $F_{(1,140, 17.10)} = 3.252$) and duration (sham: $p = 0.3044$, $F_{(1,472, 25.03)} = 1.202$; 3-months post LIB: $p = 0.073$, $F_{(1,081, 16.22)} = 3.606$) of mEPSCs in sham controls and LIB-exposed mice at 3-months post injury (Fig. 3C and F).

3.2. Discrimination learning deficits assessed by the HCM in LIB-exposed mice at 3-months post injury

A 96-h CognitionWall task was carried out in mice at 3-months post injury to investigate the long-term consequences of cognitive function by LIB exposure. Experimental timeline and devices are illustrated in Fig. 4A and B. The CognitionWall has three entrances placed in front of a food dispenser in the automated PhenoTyper home-cage. Mice entering

the designated entrance five times obtained one food pellet as a reward. No rewards were obtained when mice entered the other two entrances. Initially, frequencies of entering the three entrances were assessed to establish pre-experimental preferences. No significant preference for the setting of the CognitionWall entrances was identified during the first 30 entries (Fig. 4C) in both LIB-exposed mice and sham controls. To exclude the possibility that different performances in the CognitionWall tasks were caused by differences in overall locomotor activity, the total distance traveled during the 4-day experiment was calculated (Fig. 4D). In addition, total numbers of entries through any of the entrances (left, middle, and right) were calculated during the initial discrimination learning (Fig. 4E) and reversal learning phases (Fig. 4F). These locomotion and task activities in LIB-exposed mice were not significantly different from sham controls.

During the initial discrimination learning phase, mice enter through the left entrance for food pellet reward. Both LIB-exposed mice and sham controls improved their pellet earnings and fractions of correct entries on Day 2 (D2) compared with Day 1 (D1). LIB-exposed mice earned significantly fewer pellets by 13.4% (sham controls, 134.0 ± 7.490 , $n = 24$; LIB-exposed mice, 116.1 ± 6.657 , $n = 34$, $p = 0.0408$, $t = 1.773$, $df = 56$) and had significantly lower fractions of correct entries by 7.0% (sham controls, 0.7199 ± 0.01747 , $n = 24$; LIB-exposed mice, 0.6701 ± 0.01605 , $n = 34$, $p = 0.0217$, $t = 2.066$, $df = 56$) than sham controls on D1 (Fig. 5A and B). A similar trend, but no significant differences, was found on D2 of the initial discrimination learning phase.

To further assess the learning ability for this task processing, the total numbers of entries reaching specific accuracies were calculated. In this experimental procedure, an 80% criterion indicated that 24 entries out of the last 30 entries were correct as a moving window. Higher numbers of entries required to reach criteria demonstrate slower learning processing. In order to include mice that did not reach a certain learning criterion during the task, survival plots of entries reaching each criterion were plotted with log rank statistics. Separations of Kaplan–Meier

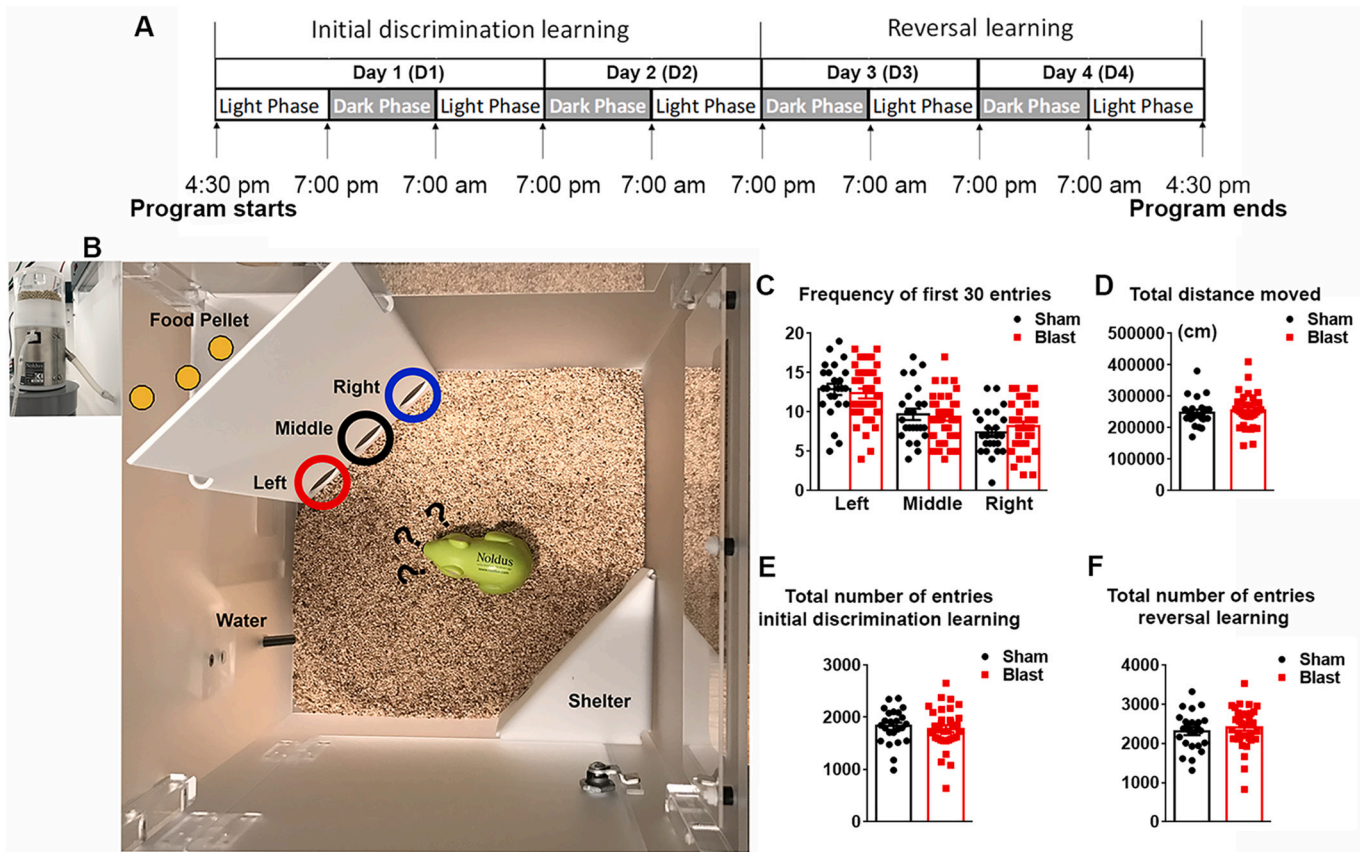


Fig. 4. Experimental setup and sequence for CognitionWall behavioral testing.

Timeline of experiments (A) and depiction of the PhenoTyper layout (B) with the CognitionWall. Numbers of entries through *left*, *middle* and *right* entrance during the first 30 entries after protocol starts (C). Total distance moved during the 4-day CognitionWall testing (D). Total number of entries during the initial discrimination learning phase (E) and reversal learning phase (F) through any of the entrances (*left*, *middle* and *right*).

survival curves between LIB-exposed mice and sham controls could be identified reaching criteria of 80–90%; statistically significant differences between LIB-exposed mice and sham controls occurred in 83% ($p = 0.0276$) and 87% criteria ($p = 0.0081$) (Fig. 5C to F). The significantly lower accuracies, fewer food rewards earned and more entries required to reach certain performance indicate impairment of discrimination learning ability in LIB-exposed mice.

3.3. Cognitive flexibility deficits for learning process assessed by the HCM in LIB-exposed mice at 3-months post injury

After the 2-day initial discrimination learning, an automated reversal learning test was implemented in the same CognitionWall device through the pre-programmed setting on Day 3 (D3) and 4 (D4). To assess cognitive flexibility during the reversal learning phase, mice were examined on passing through the *right* entrance to obtain food pellets. Mice have to extinguish the previous reward paradigm and generate a new one (Logan et al., 2019). Both LIB-exposed mice and sham controls improved on reward earnings and fractions of correct entries on D4 compared with D3. While the pellets earned by LIB-exposed mice did not significantly differ from that of the sham controls on both D3 and D4 of the reversal learning phase (Fig. 6A), LIB-exposed mice had significantly lower fractions of correct entries by 9.2% (sham controls, 0.7591 ± 0.01856 , $n = 24$; LIB-exposed mice, 0.6890 ± 0.01552 , $n = 34$, $p = 0.0027$, $t = 2.899$, $df = 56$) than sham controls on D4 but not D3 of the reversal learning phase (Fig. 6B). The number of entries through the previously correct entry (*left*) were measured as perseverative errors; the number of entries through the non-reward entry (*middle*) were measured as neutral errors (Rommelink et al., 2016b). LIB-exposed mice had

significantly more perseverative errors than sham controls ($p = 0.0235$, $F_{(1, 56)} = 5.424$). 45.5% more perseverative errors were observed in LIB-exposed mice compared to sham controls on D4 of the reversal learning phase (sham controls, 196.1, $n = 24$; LIB-exposed mice, 285.4, $n = 34$, SE of difference 31.37, $p < 0.05$), while no significant differences on D3 (Fig. 6C). The numbers of neutral errors were not significantly different between two groups ($p = 0.3045$, $F_{(1, 56)} = 1.074$) (Fig. 6D) on both days of the reversal learning phase.

Separations of Kaplan–Meier survival curves between LIB-exposed mice and sham controls could be identified reaching criteria of 80–90%; statistically significant differences between LIB-exposed mice and sham controls occurred in 87% ($p = 0.0477$) (Fig. 6E to H). The significant lower accuracies, more perseverative errors, and more entries required to reach certain performance indicate impairment of cognitive flexibility in the LIB-exposed mice.

3.4. Patterns of learning deficits assessed by the HCM in LIB exposed mice at 3-months post injury

The frequency of *left* entries during the 96-h testing was calculated hourly in order to assess dynamic patterns of learning ability in LIB-exposed mice and sham controls. Most of the entries were performed in dark phase. LIB-exposed mice performed poorly from the 4th to 9th hour (duration of 6 h, blue dot square in Fig. 7A) during the initial discrimination learning phase. After the 9th hour, the two groups performed comparably. During the reversal learning phase, the *left* entries were considered perseverative errors. Both groups mainly made *left* entries on D3, indicating slow cognitive set switch. Sham control mice performed better during the entire dark phase of D4 (from the 75th to

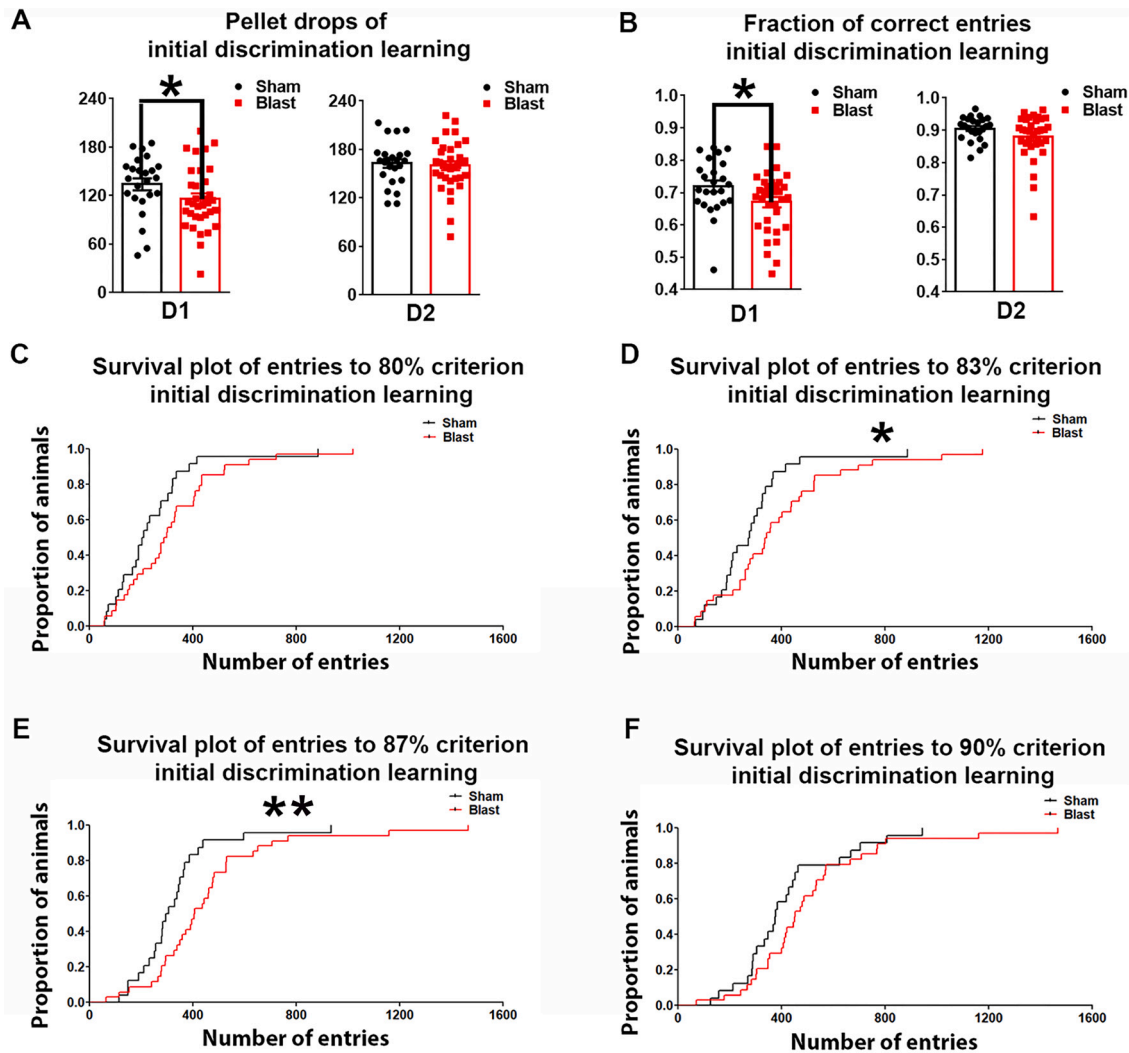


Fig. 5. Discrimination learning performance assessed by the HCM system.

Total numbers of pellets (food rewards) earned during the initial discrimination learning phase (A). Numbers of entries made through correct entrance (left) during initial learning phase, divided by total numbers of entries, providing a proportion of correct entries (B). *, $p < 0.05$ by one-tailed, unpaired Student's t -test. Survival plot of entries to different criteria during the initial discrimination learning phase (C–F). Kaplan–Meier plot of discrimination learning performance in sham controls and LIB-exposed mice achieving 80% (C), 83% (D), 87% (E), and 90% (F) criteria. This plot showed the proportions of mice reaching criterion (y-axis) at a given total number of entries (x-axis). * $p < 0.05$ and ** $p < 0.01$ by Log-rank (Mantel-Cox) test.

87th hour, duration of 12 h, blue dot square in Fig. 7A) compared with LIB-exposed mice, indicating mild but prolonged cognitive flexibility deficits of LIB-exposed mice. With continuous evaluation of the performance between specific entries, we observed similar patterns such that a significant difference was identified starting at 100 entries but merged by 800 entries during the initial discrimination learning phase ($p = 0.0282$, $F_{(1, 54)} = 5.084$); the predominant difference was between 350 and 400 entries ($p < 0.05$) (Fig. 7B). In the meantime, a trend of poorer performance of LIB-exposed mice was identified from the 500 entries and persisted after the 1200 entries during the reversal learning phase ($p = 0.1099$, $F_{(1, 55)} = 2.640$ for Fig. 7C).

In a previous study, no correlation between performance in initial discrimination learning and reversal learning tasks was found in non-injured adult C57BL/6J mice (Remmelink et al., 2016b). Here, we investigated whether the performance on D1 of the initial discrimination learning phase was associated with the performance on D4 of the reversal learning phase (Fig. 8A). Interestingly, no significant correlation was found in sham control mice between the performance in the initial discrimination phase and reversal learning tasks ($p = 0.4335$, Fig. 8B), consistent as previously reported in non-injured adult C57BL/

6J mice. In contrast, a weak but statistically significant positive correlation was found in LIB-exposed mice ($p = 0.0158$, $r = 0.4110$, Fig. 8C), indicating a possible prediction of the performance in LIB-exposed mice on different types of learning deficits.

3.5. Quantitative analysis of hippocampal global-proteome profiles using data-independent acquisition in LIB-exposed mice at 3-months post injury

To investigate molecular processes of glutamate hyperexcitability affecting long-term cognitive deficits in mice exposed to LIB exposure, profiles of global-proteomes in mouse hippocampus at 3-months post injury were analyzed using label-free quantitative mass spectrometry. As a next-generation proteomic methodology, the DIA strategy was used to exhibit much higher sensitivity and reproducibility compared with the conventional DDA approach (Krasny and Huang, 2021). We identified 5354 proteins in the hippocampus of LIB-exposed mice and sham controls (Fig. 9A). Proteins with a p -value less than 0.05, fold change larger than 1.3, and intensity over 3000 were considered significant changes. Among 5354 proteins, 43 proteins were identified with a significant difference between LIB-exposed mice and sham controls.

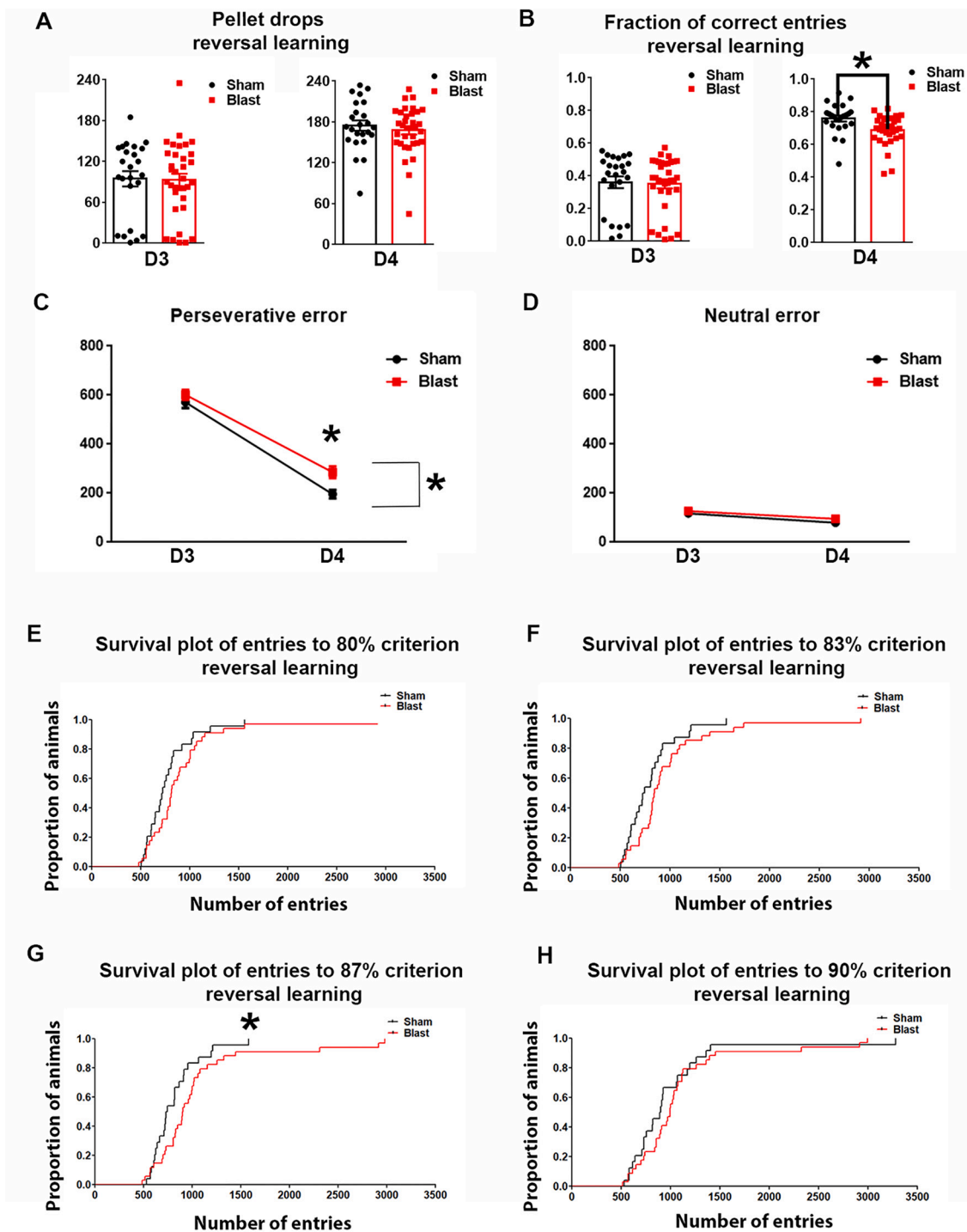


Fig. 6. Cognitive flexibility for learning process assessed by the HCM system.

Total numbers of pellets (food rewards) earned during reversal learning phase (A). Numbers of entries through correct entrance (right) during reversal phase, divided by the total numbers of entries, providing a proportion of correct entries (B). Numbers of perseverative errors (left entry) (C) and neutral errors (middle entry) (D) during reversal learning phase. * $p < 0.05$ by one-tailed, unpaired Student's *t*-test. Survival plot of entries to different criteria during reversal learning (E-H). Kaplan–Meier plot of discrimination learning performance in sham controls and LIB-exposed mice achieving 80% (E), 83% (F), 87% (G), and 90% (H) criteria. This plot showed the proportions of mice reaching criterion (y-axis) at a given total number of entries (x-axis). * $p < 0.05$ by Log-rank (Mantel-Cox) test.

Among them, 28 proteins showed significantly lower expression; and 15 proteins showed significantly higher expression in the hippocampus of LIB-exposed mice compared with sham controls (Table 1). Proteins with a significant difference were further examined on the STRING database to evaluate the protein-protein interaction networks. A cluster of 6 proteins associated with serine protease inhibitors (SERPINS) showed

high confidence interactions with interaction scores > 0.7 , including alpha-1-antitrypsin 1-2 (Serpina1b), alpha-1-antitrypsin 1-4 (Serpina1d), alpha-1-antitrypsin 1-5 (Serpina1e), antithrombin-III (Serpinc1), vimentin (Vim) and fibronectin (Fn1). All SERPIN-related proteins were higher expressed in LIB-exposed mice compared with sham controls. In addition, another protein in the SERPIN family, serine protease inhibitor

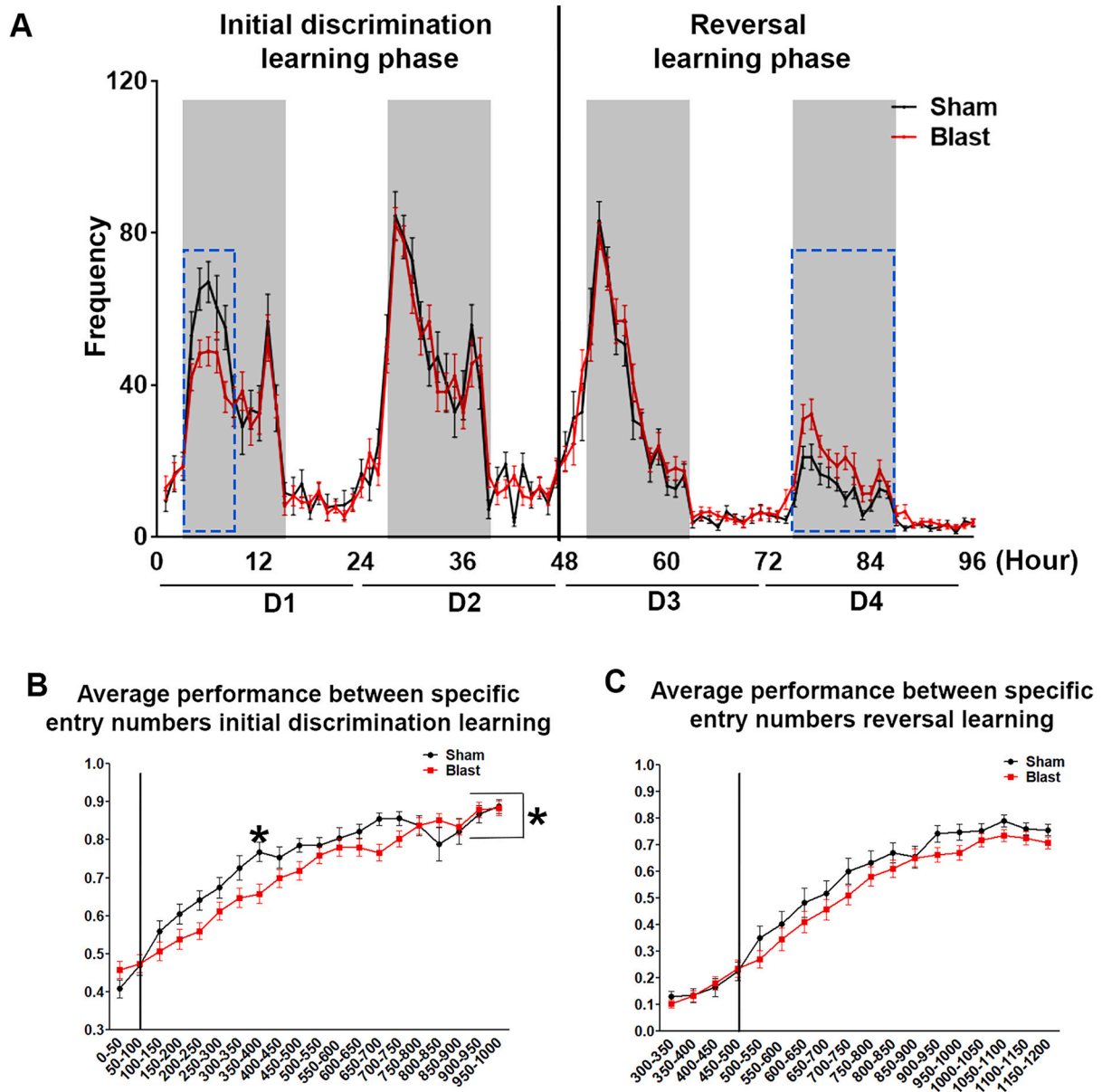


Fig. 7. Dynamic patterns of learning deficits assessed by the HCM system.

Frequency of left entries for food pellet rewards during the 96-h experimental period of the CognitionWall task (A). Data acquisition was continuously during both the light and dark phases. Gray shadow represents the dark phase. The blue dotted lines show the duration of observed differences between sham controls and LIB-exposed mice. The average fractions of the correct entrances between specific entry numbers during the initial discrimination learning (B) and reversal learning phase (C). * $p < 0.05$ by two-way ANOVA using Bonferroni post-tests. (For interpretation of the references to colour in this figure legend, the reader is referred to the web version of this article.)

A3K (Serpina3k), was also upregulated in LIB-exposed mice (Fig. 9B). The fold changes of these SERPIN-related proteins were ranging from 1.36 to 1.86 (Fig. 9C). In further comparing peer-reviewed research articles (Aber et al., 2003; Caroni et al., 2012; Chédotal, 2007; Fasolino and Zhou, 2017; Glasgow et al., 2021; Jaworski et al., 2019; Kaltschmidt and Kaltschmidt, 2015; Lim et al., 2001; Makani et al., 2012; Weber et al., 2019), 6 proteins involved in synaptic plasticity and cognitive function were downregulated in LIB-exposed mice, including netrin-G1 (Ntng1), slit homolog 1 protein (Slit1), protein phosphatase 1 regulatory subunit 3F (Ppp1r3f), GSK3B-interacting protein (Gskip), ankyrin repeat domain-containing protein 40 (Ankrd40) and methyl-CpG-binding domain protein 2 (Mbd2) with fold changes ranging from 0.62 to 0.75. Carbonic anhydrase 14 (Ca14) and nuclear factor NF-kappa-B p105 subunit (Nfkb1) were upregulated with fold changes ranging

from 1.33 to 1.62 (Fig. 9D). This high-sensitivity proteomic analysis indicates that the impairment of synaptic plasticity is associated with SERPINs in mice exposed to LIB in the chronic phase.

3.6. Association studies of alteration of proteomic profiles in hippocampus with learning deficits assessed by the HCM in LIB exposed mice at 3-months post injury

A regression approach was used to determine whether these 7 affected proteins associated with SERPINs and whether 8 affected proteins involving synaptic plasticity and cognitive function correlated with the cognitive learning function assessed by the HCM. Pearson's r -values ≤ -0.3 or ≥ 0.3 were considered of correlation in this study. Correlations of performance on D1 of the initial discrimination learning phase

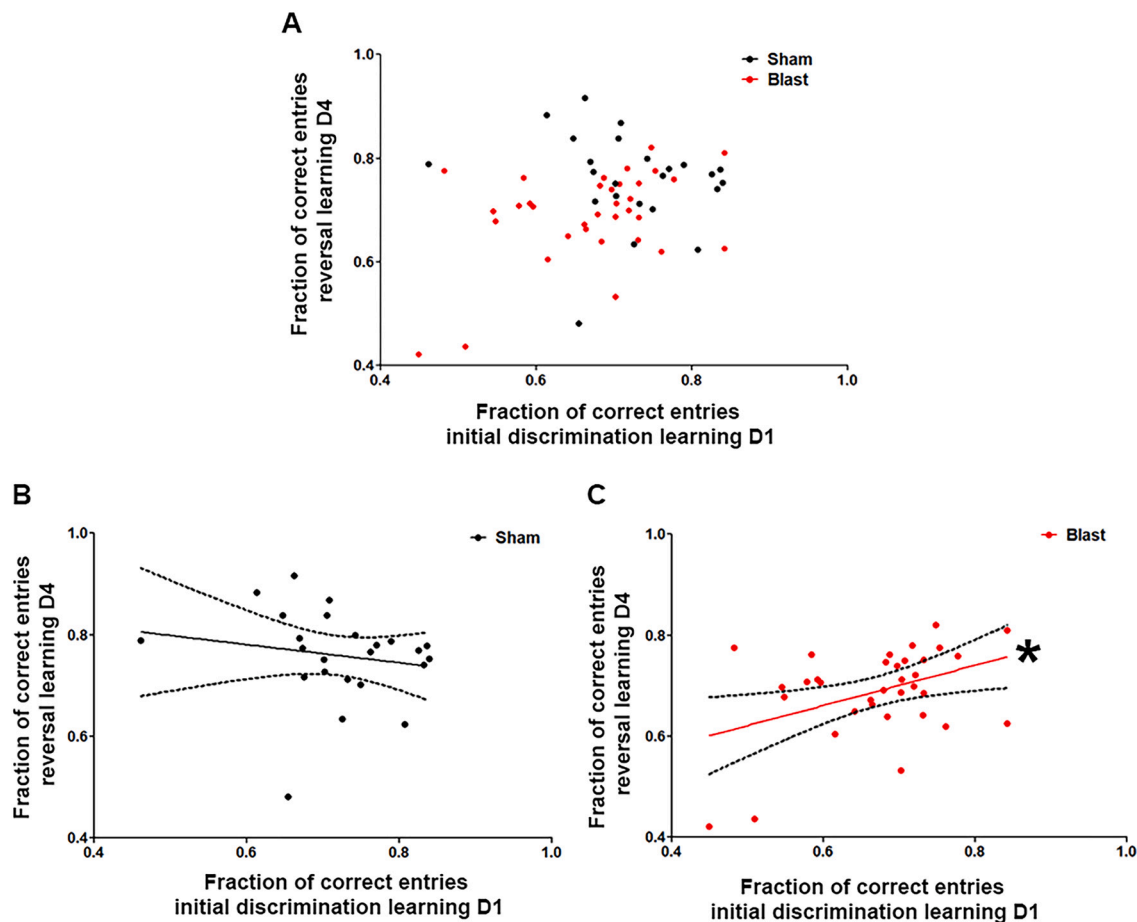


Fig. 8. Correlation between the performance in the initial discrimination and reversal learning tasks. Fractions of correct entries on D1 of initial discrimination learning phase vs. on D4 of reversal learning phase were plotted (A) with the regression lines drawn in solid lines and the dotted curves for 95% confidence intervals in sham controls (B) and LIB-exposed mice (C). * $p < 0.05$, $r = 0.4110$.

and DIA protein intensity showed ankyrin repeat domain-containing protein 40 and GSK3B-interacting protein exhibited positive correlations; while carbonic anhydrase 14, nuclear factor NF-kappa-B p105 subunit, antithrombin-III and vimentin exhibited negative correlations (Fig. 10A). Correlations of performance on D4 of the reversal learning phase and DIA protein intensity showed methyl-CpG-binding domain protein 2 exhibited positive correlations; while carbonic anhydrase 14 and vimentin exhibited negative correlations (Fig. 10B). Other proteins with Pearson's r -values ranging -0.3 to 0.3 are summarized in Supplemental Figs. 4 and 5.

4. Discussion

Our previous studies demonstrated that a single open-field LIB exposure with a peak overpressure at 46.6 kPa and a maximal impulse of 60 kPa \times ms (Rutter et al., 2021) resulted in increased asymmetric excitatory synapses in mouse hippocampus at 7- and 30-days post injury using transmission electron microscopy (TEM) quantification (Konan et al., 2019). These findings encouraged further research on characterizing changes in neural activity and synaptic consequences following LIB exposure. In this study, we first evaluated neuronal electrophysiology in individual neurons in hippocampal CA3 region involving synaptic plasticity, cognitive function and memory processes (Cherubini and Miles, 2015). We found that a single LIB exposure significantly increased the frequencies of mEPSCs in mice at both 1- and 7-days post injury without altering the amplitudes of mEPSCs. Furthermore, mEPSCs recorded from LIB-exposed mice displayed a burst pattern. Bath

application of NMDAR antagonist reduced the frequencies and eliminated the burst pattern of glutamatergic mEPSCs without changing their amplitudes. Because presynaptic NMDARs are relatively insensitive to Mg^{2+} blockade at resting membrane potentials (Mayer et al., 1984), these data suggest that presynaptic NMDARs likely play predominant roles in enhanced glutamatergic synaptic inputs to hippocampal neurons in response to LIB exposure, while the involvement of postsynaptic NMDARs cannot be completely ruled out (Kunz et al., 2013; McGuinness et al., 2010; Prius-Mengual et al., 2019; Savtchouk et al., 2019). Though the average level of hyperactivity was not significantly different between LIB-exposed mice at 3-months post injury and sham controls, the frequencies of mEPSCs, numbers and duration of burst mEPSCs varied between individual neurons. Some neurons showed decreased hyperactive patterns at 3-months post LIB compared to those at 1-day and 7-days post LIB. It is possible that these neurons undergo adaptations and achieve synaptic homeostasis (Kim and Tsien, 2008; Macleod and Zin-smaier, 2006). It is also possible that prolonged excitotoxicity affects structures, functions and survivals of neuronal cells (Lewerenz and Maher, 2015). This possibility is supported by our bioinformatic analysis findings demonstrating that proteins related to synaptic plasticity were altered in the hippocampal tissues at 3-months post LIB.

The primary blast shockwaves cause micro/nano-scale intracellular damage of cytoskeleton, ion channel proteins, and cell adhesion molecules without apparent neuropathology on cell death and astrogliosis response (Gao et al., 2011; Hemphill et al., 2015; Monnerie et al., 2010; Park and Biederer, 2013; Przekwas et al., 2016; Song et al., 2018a; Song et al., 2018b). Our previous study indicates that exposure to a single

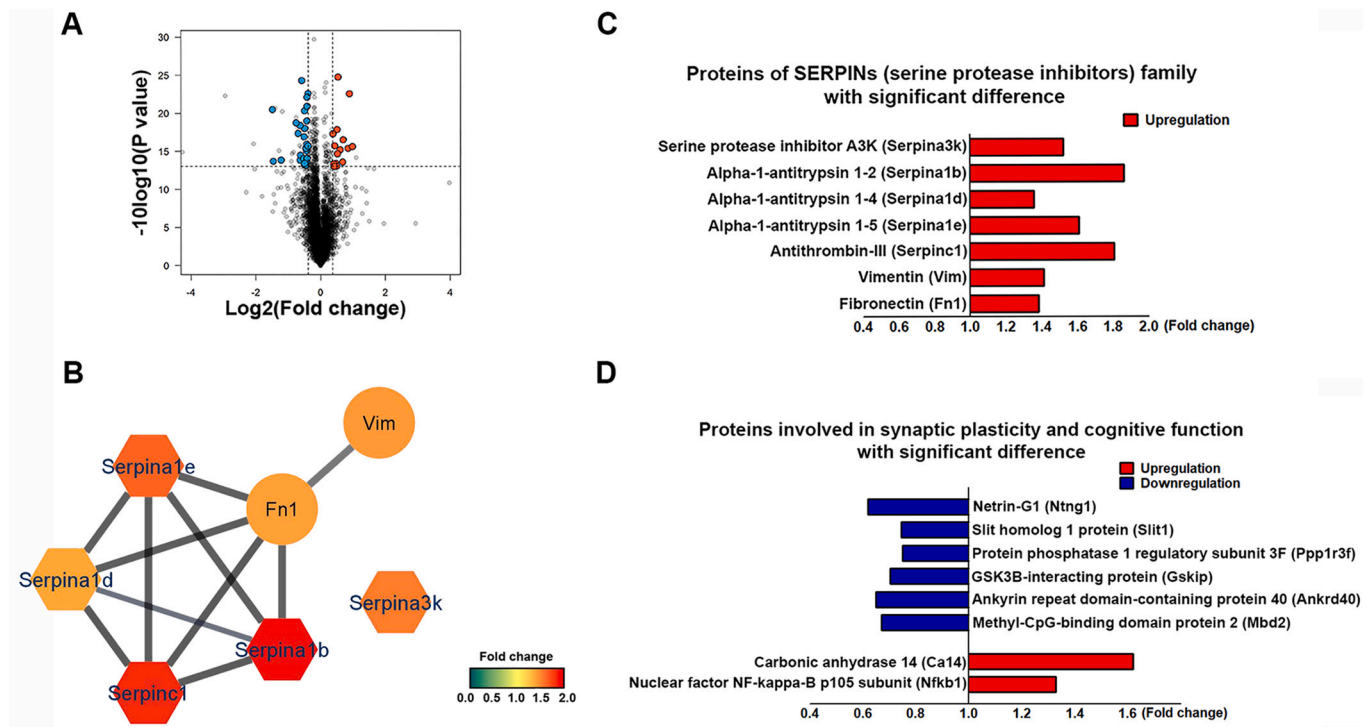


Fig. 9. Hippocampal global-proteome profiles using data-independent acquisition.

Volcano plot showing the significant protein variation between sham controls and LIB-exposed mice. Statistical analysis was performed by unpaired two-tailed Student t-test. A statistical significance was considered by p -value < 0.05 , fold change > 1.3 -fold and at least three samples per group having intensity ≥ 3000 . Red dots indicate proteins having significant increases. Blue dots show proteins having significant decreases. Gray dots indicate proteins not meeting criteria (A). Protein interaction network of significant proteins between sham controls and LIB-exposed mice. Six proteins show high confidence interactions with interaction scores > 0.7 . The five hexagon nodes represent proteins with conserved SERPIN domain. The colour of the nodes represents the protein intensity ratio between sham controls and LIB-exposed mice (B). Fold changes of proteins with significant difference related to SERPINs (serine protease inhibitors) (C). Fold changes of proteins with significant difference related to synaptic plasticity and cognitive function (D). (For interpretation of the references to colour in this figure legend, the reader is referred to the web version of this article.)

blast also significantly alters phosphorylated proteins involved in maintaining microtubule stability and axonal integrity (Chen et al., 2018). In addition, LIB exposure upregulates phosphorylated proteins involved in regulating Ca^{2+} hemostasis, such as calcium/calmodulin-dependent protein kinase type II subunit beta (CaMKIIb), plasma membrane calcium-transporting ATPase 1 (Atp2b1) and synaptotagmin I (Syt1) (Chen et al., 2018). Upregulation of phosphorylated proteins may be responsible for presynaptic NMDAR-dependent transmitter release (Kunz et al., 2013). Neuroinflammation also plays important roles in hyperexcitability post TBI (Mayeux et al., 2017; Mukherjee et al., 2020; Webster et al., 2017). Mild TBI in mice from a weight-drop model leads to pro-inflammatory responses in microglia and increased excitatory inputs in the acute phase post injury (Witkowski et al., 2019). Blast exposure was demonstrated contributing to oxidative stress and inflammatory changes in our previous study and others, mainly in the acute phase post injury (Elder et al., 2015; Song et al., 2019; Sosa et al., 2017).

Glutamate release following TBI may lead to multiple short- and long-term excitatory injuries. In the acute phase, excessive glutamate triggers ions influx, oxidative stress, and mitochondrial dysfunction, resulting in neuronal cell death, injury or dysfunction, as well as impaired neuroplasticity. In the subacute and chronic phases of excitatory injuries, compensatory changes against glutamate excitotoxicity will lead to receptor alteration, dysregulated excitatory-inhibitory balance and maladaptive circuits, leading to neurobehavioral deficits (Dong et al., 2009; Guerriero et al., 2015). It appears that LIB exposure likely changes the intrinsic properties of NMDARs and/or a synaptic network involved in presynaptic glutamate release. Glutamate, particularly NMDAR-dependent synaptic hyperexcitability also plays

important roles in the disease progression in Alzheimer's dementia (Ghatak et al., 2019; Šišková et al., 2014). Delineating the neurological outcomes of glutamate hyperexcitability clearly provides a rationale for developing a strategy to prevent LIB-induced chronic complications.

Hippocampus plays an essential role in the processing of discrimination learning and cognitive flexibility (Frankland et al., 1998; Levick et al., 2018; Rubin et al., 2014; Teng et al., 2000), with the involvement of other brain regions, such as striatum (Fidalgo et al., 2012; Okada et al., 2014). It was reported that protein distributions and expressions in hippocampal CA3 neurons were correlated with performance on discrimination learning (Maurer et al., 2017; Olds et al., 1990). Although being well established for clinical applications, learning and memory tests in animal models are limited by unintended bias of experimenters, motivational issues, stress, and circadian shifts during light-dark cycles among others (Logan et al., 2018). Using conventional memory assessments, such as the Barnes maze and Morris Water-maze, nocturnal rodents are commonly tested during the light phase. Stresses generated during tasks increase serum corticosterone levels which impact the outcomes of memory tests (Harrison et al., 2009). Due to these confounding factors, conventional learning and memory tests may not be sufficiently sensitive to detect mild cognitive deficits induced by experimental LIB exposure. In this research we used a stress-free, automated HCM approach to access subtle changes in cognitive learning functions (Richter, 2020; Voikar and Gaburro, 2020). To minimize the disrupted pheromone sensing when animals were placed in a novel environment (Rosenbaum et al., 2009), mice in the present study were kept in the same home-cage for 72 consecutive hours prior to CognitionWall tasks. Following acclimation, CognitionWall tasks started automatically and processed pre-calibrated experimental protocols in

Table 1
Proteins altered significantly between LIB-exposed mice and sham controls.

| Genes | Protein description | Blast/Sham | Pval |
|-----------|---|------------|---------|
| Fkbp1 | FK506-binding protein-like | 0.35677734 | 0.00895 |
| Swi5 | DNA repair protein SWI5 homolog | 0.36409045 | 0.04263 |
| Tbkbp1 | TANK-binding kinase 1-binding protein 1 | 0.43212068 | 0.04128 |
| Fam241b | Protein FAM241B | 0.59262255 | 0.01338 |
| Ntng1 | Netrin-G1 | 0.61928552 | 0.01845 |
| Txndc9 | Thioredoxin domain-containing protein 9 | 0.64794245 | 0.0145 |
| Ankrd40 | Ankyrin repeat domain-containing protein 40 | 0.64851367 | 0.04122 |
| Map3k10 | Mitogen-activated protein kinase kinase kinase 10 | 0.65467438 | 0.03564 |
| Mbd2 | Methyl-CpG-binding domain protein 2 | 0.67023265 | 0.00373 |
| Znf598 | E3 ubiquitin-protein ligase ZNF598 | 0.69814627 | 0.03945 |
| Gskip | GSK3B-interacting protein | 0.70330662 | 0.02033 |
| Angel2 | Protein angel homolog 2 | 0.70915043 | 0.04742 |
| Rnf11 | RING finger protein 11 | 0.71304388 | 0.04552 |
| Pnkd | Probable hydrolase PNKD | 0.71379093 | 0.0093 |
| Phkg1 | Phosphorylase b kinase gamma catalytic chain | 0.71425415 | 0.0158 |
| Cnot3 | CCR4-NOT transcription complex subunit 3 | 0.73091601 | 0.02888 |
| Emc7 | ER membrane protein complex subunit 7 | 0.73369842 | 0.04791 |
| Akr1b7 | Aldo-keto reductase family 1 member B7 | 0.74090033 | 0.03122 |
| Bag2 | BAG family molecular chaperone regulator 2 | 0.74269498 | 0.02547 |
| Slit1 | Slit homolog 1 protein | 0.74459478 | 0.04269 |
| Wwc2 | Protein WWC2 | 0.74673017 | 0.01258 |
| Adar | Double-stranded RNA-specific adenosine deaminase | 0.74889685 | 0.00618 |
| Ppp1r3f | Protein phosphatase 1 regulatory subunit 3F | 0.74992702 | 0.00811 |
| Gcc2 | GRIP and coiled-coil domain-containing protein 2 | 0.751871 | 0.03912 |
| Gigyf1 | GRB10-interacting GYF protein 1 | 0.7537766 | 0.03911 |
| Mrpl28 | 39S ribosomal protein L28, mitochondrial | 0.76530137 | 0.02694 |
| Cyld | Ubiquitin carboxyl-terminal hydrolase CYLD | 0.76711376 | 0.00551 |
| Elac2 | Zinc phosphodiesterase ELAC protein 2 | 0.76941795 | 0.03405 |
| Eml1 | Echinoderm microtubule-associated protein-like 1 | 1.30425179 | 0.01867 |
| Nfkb1 | Nuclear factor NF-kappa-B p105 subunit | 1.32976837 | 0.04636 |
| Opalin | Opalin | 1.34600516 | 0.04979 |
| Serpina1d | Alpha-1-antitrypsin 1-4 | 1.35549951 | 0.02672 |
| Fn1 | Fibronectin | 1.38328434 | 0.04554 |
| Vim | Vimentin | 1.41270788 | 0.04964 |
| Eny2 | Transcription and mRNA export factor ENY2 | 1.42529792 | 0.01638 |
| H1-2 | Histone H1.2 | 1.43751774 | 0.03413 |
| H1-5 | Histone H1.5 | 1.45363329 | 0.00334 |
| Serpina3k | Serine protease inhibitor A3K | 1.52166518 | 0.03006 |
| Serpina1e | Alpha-1-antitrypsin 1-5 | 1.60881621 | 0.04369 |
| Ca14 | Carbonic anhydrase 14 | 1.62093193 | 0.02228 |
| Serpinc1 | Antithrombin-III | 1.80683139 | 0.02888 |
| Serpina1b | Alpha-1-antitrypsin 1-2 | 1.86141408 | 0.00555 |
| Rbp4 | Retinol-binding protein 4 | 1.98627938 | 0.02734 |

Post DIA, protein identification from LIB-exposed mice and sham controls were compared with unpaired two-tailed Student t-test. Proteins with a *p*-value less than 0.05 and fold change larger than 1.3 and intensity at least 3000 was considered as a significant change.

absence of human intervention. Assessments were performed in familiar home-cages surroundings with self-paced task progression. Learning performance was monitored continuously and analyzed dynamically during 96 consecutive hours (4 days) including alternated dark and light phases. This prolonged assessment protocol enabled identification of distinct patterns of learning abilities. In addition, the automation-based analysis minimized experimental variations generated by individual experimentalists. Thus, this HCM approach provides enhanced rigorous, refinement, and reproducibility across studies.

To our knowledge, this is the first study to assess deficits of discrimination learning and cognitive flexibility in LIB-exposed mice using the automated home-cage approach. Our data demonstrated that

LIB-exposed mice displayed a decline in discrimination learning as a long-term cognitive consequence. Importantly, with 96-h consecutive monitoring, we identified that discrimination learning ability was impaired in LIB-exposed mice mainly in the early stage of the training. An additional 6 h were required for LIB-exposed mice to acquire discrimination learning successfully from the beginning of the task. Many clinical studies reported that TBI patients took significantly longer time to detect repeated targets accurately on their tasks than healthy controls, suggesting that deficits of information processing speed are associated with TBI (Battistone et al., 2008; Ozen and Fernandes, 2012). In Iraq and Afghanistan veterans, reduced processing speed is a well-recognized long-term consequence associated with bTBI history (Jurick et al., 2021). In this study, we also identified deficits of cognitive flexibility in the chronic phase post LIB exposure. In contrast to the impairment of discrimination learning, the deficits of cognitive flexibility were mainly identified in the late stage of training to a mild degree but prolonged duration (12 h). Poorer cognitive flexibility has also been identified in military service members and veterans (Huang et al., 2020). Interestingly, using an operant set-shifting test but not in home-cage environment, Matthew et al. did not identify impairment of cognitive flexibility in a blast model of high intensity (450 kPa) (Muelbl et al., 2018). For the first time, we found a significant positive correlation between deficits of discrimination learning ability and cognitive flexibility in LIB-exposed mice, that was absent in sham controls.

To identify potential biosignatures in the chronic phase post LIB exposure, we analyzed hippocampal tissues collected from the mice after the CognitionWall tasks with quantitative mass spectrometry analysis in DIA-PASEF mode with high sensitivity for protein identification. Among the 43 proteins identified of significant difference between LIB-exposed mice and sham controls, 8 proteins were demonstrated related to synaptic plasticity and cognitive function in published studies. For example, carbonic anhydrase 14 modulates NMDA receptors by regulating perisynaptic microenvironment; GSK-3 β regulates the interaction between NMDA-dependent long-term potentiation and long-term depression; ankyrin repeats are involved in PSD-95/GKAP/Shank axis binding to NMDA receptors (Jaworski et al., 2019; Lim et al., 2001; Makani et al., 2012). Serine proteases and SERPINS, such as thrombin, plasmin, neuroserpin, neuropsin, tissue recombinant plasminogen activator (tPA) and protease nexin-1 (PN-1) have been demonstrated playing important roles in synaptic plasticity and memory formation by interacting with NMDARs (Almonte and Sweatt, 2011; Baranes et al., 1998; Gingrich et al., 2000; Inoue et al., 1994; Lebeurrier et al., 2005; Luthi et al., 1997; Maggio et al., 2008; Matsumoto-Miyai et al., 2003; Nicole et al., 2001; Samson et al., 2008; Yuan et al., 2009). A delicate balance between serine proteases and SERPINS is required to maintain the appropriate function of NMDARs. In our study, seven proteins in serine protease inhibitors (SERPINS) family were identified with strong protein-protein interactions and significantly increased in LIB-exposed mice compared with sham controls. Disruptions of the serine proteases and SERPINS hemostasis may in response to NMDAR-mediated glutamatergic hyperexcitability in the hippocampus post LIB exposure.

We further explored the associations of these proteomic alterations with cognitive function impairment in LIB-exposed mice. Down-regulation of ankyrin repeat domain-containing protein 40 and GSK3B-interacting protein; upregulation of nuclear factor NF-kappa-B p105 subunit and antithrombin-III were associated with the deficits of discrimination learning in LIB-exposed mice. Upregulation of methyl-CpG-binding domain protein 2 was associated with deficits of reversal learning in LIB-exposed mice. Upregulation of carbonic anhydrase 14 and vimentin was associated with both types of cognitive deficits. These findings suggest that LIB-induced glutamatergic hyperexcitability may dysregulate the homeostasis between serine proteases and serine protease inhibitors, further disrupt neural circuits in the chronic phase of LIB exposure (Almonte and Sweatt, 2011). Further investigations of the biological process relationships between these proteins and learning deficits are warranted. In addition, most biomarkers of acute TBI will

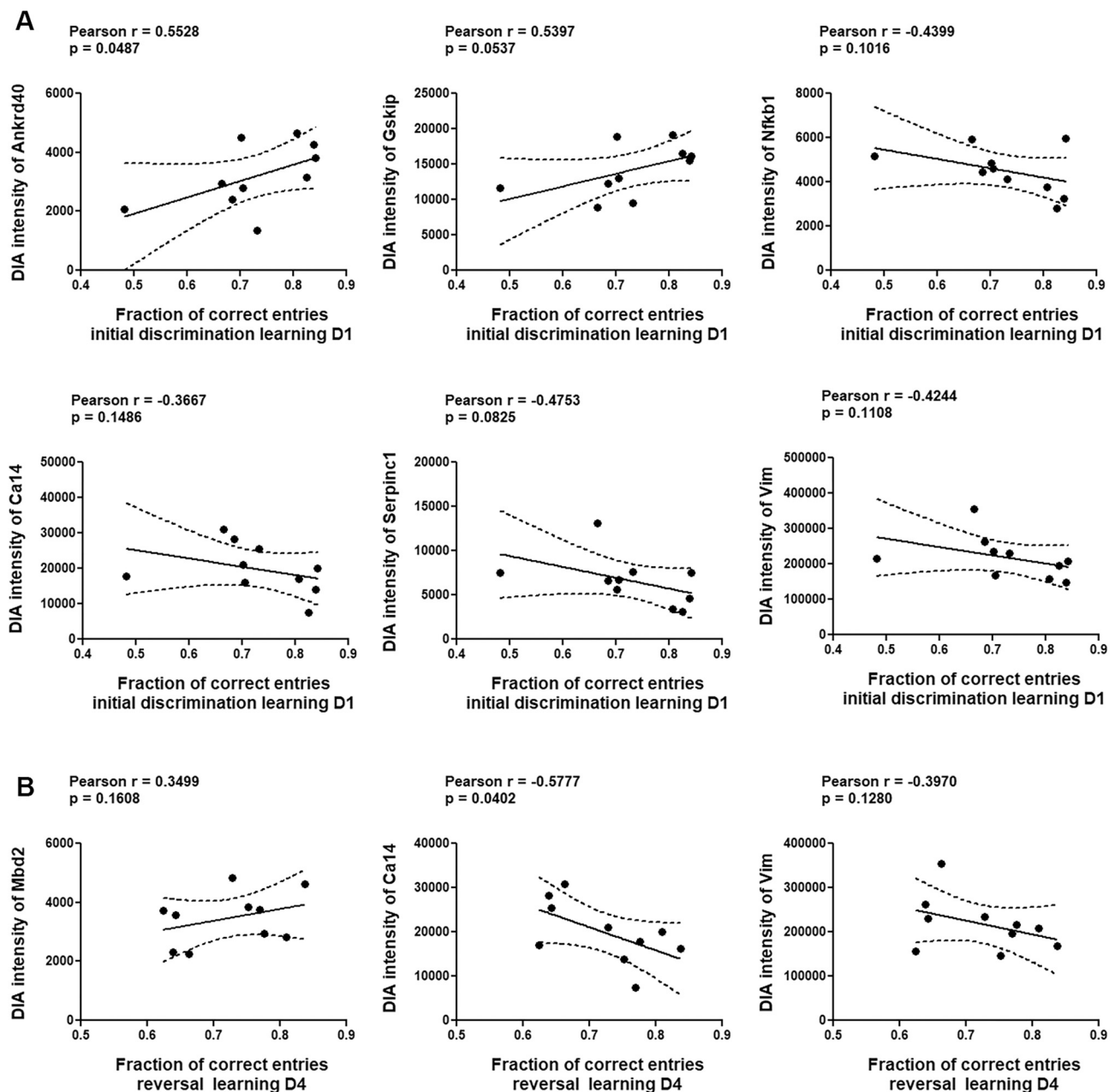


Fig. 10. Correlation analysis of significantly altered proteins in hippocampus identified by DIA with behavioral performance, Pearson's r -values ≤ -0.3 or ≥ 0.3 . Intensities of protein expression identified by DIA of significant difference vs. behavioral performance were plotted with the regression lines drawn in solid lines and the dotted curves for 95% confidence intervals. Correlation analysis of protein intensities with fractions of correct entries on Day 1 of initial discrimination learning phase (A) and on Day 4 of reversal learning phase (B) were presented with Pearson's r -values and p -values. Correlations with Pearson's r -values ≤ -0.3 or ≥ 0.3 were included in this figure.

return to baseline levels within several days following TBI, especially after mild brain injury (Wang et al., 2018). It might be appropriate to consider these proteins as potential biomarkers in the diagnosis and management of bTBI in the chronic phase following LIB exposure.

In summary, the present study demonstrates that open-field LIB exposure causes a primary brain injury. This injury is associated with the presence of hyperexcitation of glutamatergic synapses in hippocampus which are modulated by NMDARs in acute phase. Using a highly sensitive automated home-cage task, we were able to detect the impairments of discrimination learning and cognitive flexibility in the chronic phase post LIB exposure with specific patterns. Additionally, we observed altered expression of proteins that are relevant to disrupted synaptic plasticity and cognitive dysfunction in the chronic phase post

LIB exposure. Altogether, this study provides valuable information into the development of potential therapeutic targets on amelioration of hyperexcitability-modulated LIB injuries. Future studies are warranted to elucidate the precise pathophysiology pathways involved in LIB-induced glutamate hyperexcitability and enhanced presynaptic NMDAR activity. To reduce long-term neurocognitive consequences of blast-induced TBI in military service members and veterans, the present platform can be used to assess effective prevention and treatment for LIB-induced brain injuries by inhibiting glutamatergic synaptic inputs in the acute phase of LIB exposure to prevent or mitigate long-term cognitive disorders. These could include evaluating behavioral outcomes and changes of protein expressions in response to administration of NMDAR antagonists.

Supplementary data to this article can be found online at <https://doi.org/10.1016/j.nbd.2022.105634>.

CRediT authorship contribution statement

Shanyan Chen: Investigation, Formal analysis, Writing – original draft. **Heather R. Siedhoff:** Investigation, Formal analysis, Writing – original draft. **Hua Zhang:** Investigation, Formal analysis, Writing – review & editing. **Pei Liu:** Investigation, Formal analysis, Writing – review & editing. **Ashley Balderrama:** Investigation, Formal analysis, Writing – review & editing. **Runting Li:** Investigation. **Catherine Johnson:** Investigation. **C. Michael Greenleaf:** Writing – review & editing. **Bastijn Koopmans:** Resources, Writing – review & editing. **Timothy Hoffman:** Writing – review & editing. **Ralph G. DePalma:** Writing – review & editing. **De-Pei Li:** Formal analysis, Writing – review & editing. **Jiankun Cui:** Conceptualization, Project administration, Investigation, Formal analysis, Data curation, Writing – review & editing. **Zecong Gu:** Conceptualization, Supervision, Project administration, Funding acquisition, Investigation, Formal analysis, Writing – original draft.

Declaration of Competing Interest

The authors declare no competing financial interests.

Acknowledgements

The authors thank the intellectual input by Dr. Alex Chiu during the initial design of the home-cage behavioral study, and Dr. Stuart Lipton for his critical comments. This publication was made possible in part by funding from the Department of Veterans Affairs Offices of Research & Development (VA ORD) the LAMB/ShEEP programs, the BLR&D Director Service program (UFR-002-18F), Open-Field Blast (OFB) Core, and the Collaborative Merit Review for TBI Research Program (I01 BX004313-01A1); as well as the DoD Congressionally Directed Medical Research Programs (CDMRP) for the Peer Reviewed Alzheimer's Research Program Convergence Science Research Award (PRARP-CSRA; AZ180043) and the research funds of the University of Missouri (ZG); as well as by funding from NIH National Heart, Lung, and Blood Institute (R01 HL142133, R01 HL139523, and R01 HL159157 grants to DL). Its contents are solely the responsibility of the authors and do not necessarily represent the official views of the United States government, the Department of Veterans Affairs, the Department of Defense, the United States Army.

References

- Aber, K., et al., 2003. Methyl-CpG-binding protein 2 is localized in the postsynaptic compartment: an immunochemical study of subcellular fractions. *Neuroscience*. 116, 77–80.
- Agoston, D.V., 2017. Modeling the long-term consequences of repeated blast-induced mild traumatic brain injuries. *J. Neurotrauma* 34, S44–S52.
- Almonte, A.G., Sweatt, J.D., 2011. Serine proteases, serine protease inhibitors, and protease-activated receptors: roles in synaptic function and behavior. *Brain Res.* 1407, 107–122.
- Baranes, D., et al., 1998. Tissue plasminogen activator contributes to the late phase of LTP and to synaptic growth in the hippocampal mossy fiber pathway. *Neuron*. 21, 813–825.
- Battistone, M., et al., 2008. Processing speed deficits associated with traumatic brain injury: processing inefficiency or cautiousness? *Appl. Neuropsychol.* 15, 69–78.
- Belding, J.N., et al., 2021. Potential health and performance effects of high-level and low-level blast: a scoping review of two decades of research. *Front. Neurol.* 12, 274.
- Belmont Jr., P.J., et al., 2012. Combat wounds in Iraq and Afghanistan from 2005 to 2009. *J. Trauma Acute Care Surg.* 73, 3–12.
- Caroni, P., et al., 2012. Structural plasticity upon learning: regulation and functions. *Nat. Rev. Neurosci.* 13, 478–490.
- Chédotal, A., 2007. Slits and their receptors. *Axon Growth Guid.* 65–80.
- Chen, M., et al., 2018. Proteomic profiling of mouse brains exposed to blast-induced mild traumatic brain injury reveals changes in axonal proteins and phosphorylated tau. *J. Alzheimers Dis.* 66, 751–773.
- Cherubini, E., Miles, R.M., 2015. The CA3 region of the hippocampus: how is it? What is it for? How does it do it? *Front. Cell. Neurosci.* 9, 19.
- da Veiga Leprevost, F., et al., 2020. Philosopher: a versatile toolkit for shotgun proteomics data analysis. *Nat. Methods* 17, 869–870.
- Demichev, V., et al., 2021. High sensitivity dia-PASEF proteomics with DIA-NN and FragPipe. *bioRxiv*, 2021.03.08.434385. <https://www.biorxiv.org/content/10.1101/2021.03.08.434385v1.full>.
- DePalma, R.G., Hoffman, S.W., 2018. Combat blast related traumatic brain injury (TBI): decade of recognition; promise of progress. *Behav. Brain Res.* 340, 102–105.
- Deuker, L., et al., 2014. Human neuroimaging studies on the hippocampal CA3 region—integrating evidence for pattern separation and completion. *Front. Cell. Neurosci.* 8, 64.
- Dong, X.-X., et al., 2009. Molecular mechanisms of excitotoxicity and their relevance to pathogenesis of neurodegenerative diseases. *Acta Pharmacol. Sin.* 30, 379–387.
- Dorsett, C.R., et al., 2017. Glutamate neurotransmission in rodent models of traumatic brain injury. *J. Neurotrauma* 34, 263–272.
- Elder, G.A., et al., 2015. Vascular and inflammatory factors in the pathophysiology of blast-induced brain injury. *Front. Neurol.* 6, 48.
- Engel, C.C., et al., 2019. The Neurological Effects of Repeated Exposure to Military Occupational Blast: Implications for Prevention and Health: Proceedings, Findings, and Expert Recommendations from the Seventh Annual Department of Defense State-of-the-Science Meeting, 12–14 March, 2018. RAND, Santa Monica, CA xvi, 90 pages.
- Fasolino, M., Zhou, Z., 2017. The crucial role of DNA methylation and MeCP2 in neuronal function. *Genes*. 8, 141.
- Fidalgo, C., et al., 2012. Functional interaction between the dorsal hippocampus and the striatum in visual discrimination learning. *J. Neurosci. Res.* 90, 715–720.
- Frankland, P.W., et al., 1998. The dorsal hippocampus is essential for context discrimination but not for contextual conditioning. *Behav. Neurosci.* 112, 863.
- Frautschy, S.A., Cole, G.M., 2010. Why pleiotropic interventions are needed for Alzheimer's disease. *Mol. Neurobiol.* 41, 392–409.
- Gao, X., et al., 2011. Moderate traumatic brain injury causes acute dendritic and synaptic degeneration in the hippocampal dentate gyrus. *PLoS One* 6, e24566.
- Ghatak, S., et al., 2019. Mechanisms of hyperexcitability in Alzheimer's disease hiPSC-derived neurons and cerebral organoids vs isogenic controls. *Elife*. 8, e50333.
- Gingrich, M.B., et al., 2000. Potentiation of NMDA receptor function by the serine protease thrombin. *J. Neurosci.* 20, 4582–4595.
- Glasgow, S.D., et al., 2021. Guiding synaptic plasticity: novel roles for netrin-1 in synaptic plasticity and memory formation in the adult brain. *J. Physiol.* 599, 493–505.
- Guerrero, R.M., et al., 2015. Glutamate and GABA imbalance following traumatic brain injury. *Curr Neurol Neurosci Rep.* 15, 27.
- Harrison, F.E., et al., 2009. Endogenous anxiety and stress responses in water maze and Barnes maze spatial memory tasks. *Behav. Brain Res.* 198, 247–251.
- Hemphill, M.A., et al., 2015. Traumatic brain injury and the neuronal microenvironment: a potential role for neuropathological mechanotransduction. *Neuron*. 85, 1177–1192.
- Huang, M.X., et al., 2020. Marked increases in resting-state MEG gamma-band activity in combat-related mild traumatic brain injury. *Cereb. Cortex* 30, 283–295.
- Inoue, K., et al., 1994. Modulatory effect of plasminogen on NMDA-induced increase in intracellular free calcium concentration in rat cultured hippocampal neurons. *Neurosci. Lett.* 179, 87–90.
- Jaber, S.M., et al., 2014. Dose regimens, variability, and complications associated with using repeat-bolus dosing to extend a surgical plane of anesthesia in laboratory mice. *J. Am. Assoc. Lab. Anim. Sci.* 53, 684–691.
- Jaworski, T., et al., 2019. GSK-3beta at the intersection of neuronal plasticity and neurodegeneration. *Neural Plast.* 2019, 4209475.
- Jurick, S.M., et al., 2021. Independent and synergistic associations between TBI characteristics and PTSD symptom clusters on cognitive performance and Postconcussive symptoms in Iraq and Afghanistan veterans. *J. Neuropsychiatr. Clin. Neurosci.* 33(2), 98–108.
- Kaltschmidt, B., Kaltschmidt, C., 2015. NF-KappaB in long-term memory and structural plasticity in the adult mammalian brain. *Front. Mol. Neurosci.* 8, 69.
- Kennedy, M.B., 2013. Synaptic signaling in learning and memory. *Cold Spring Harb. Perspect. Biol.* 8, a016824.
- Kim, J., Tsien, R.W., 2008. Synapse-specific adaptations to inactivity in hippocampal circuits achieve homeostatic gain control while dampening network reverberation. *Neuron*. 58, 925–937.
- Konan, L.M., et al., 2019. Multi-focal neuronal Ultrastructural abnormalities and synaptic alterations in mice after low-intensity blast exposure. *J. Neurotrauma* 36, 2117–2128.
- Kong, A.T., et al., 2017. MSFragger: ultrafast and comprehensive peptide identification in mass spectrometry-based proteomics. *Nat. Methods* 14, 513–520.
- Kovacevic, J., et al., 2018. Protein instability, haploinsufficiency, and cortical hyperexcitability underlie STXBPI encephalopathy. *Brain*. 141, 1350–1374.
- Krasny, L., Huang, P.H., 2021. Data-independent acquisition mass spectrometry (DIA-MS) for proteomic applications in oncology. *Mol Omics*. 17, 29–42.
- Kucherov, Y., et al., 2012. Blast induced mild traumatic brain injury/concussion: a physical analysis. *J. Appl. Phys.* 112, 104701.
- Kunz, P.A., et al., 2013. Presynaptic NMDA receptor mechanisms for enhancing spontaneous neurotransmitter release. *J. Neurosci.* 33, 7762–7769.
- Lebeurrier, N., et al., 2005. The brain-specific tissue-type plasminogen activator inhibitor, neuroserpin, protects neurons against excitotoxicity both in vitro and in vivo. *Mol. Cell. Neurosci.* 30, 552–558.
- Levcik, D., et al., 2018. The role of the hippocampus in object discrimination based on visual features. *Neurobiol. Learn. Mem.* 155, 127–135.
- Lewerenz, J., Maher, P., 2015. Chronic glutamate toxicity in neurodegenerative diseases—what is the evidence? *Front. Neurosci.* 9, 469.

- Li, D.P., et al., 2017. CaMKII regulates synaptic NMDA receptor activity of hypothalamic Presympathetic neurons and sympathetic outflow in hypertension. *J. Neurosci.* 37, 10690–10699.
- Lim, S., et al., 2001. Sharpin, a novel postsynaptic density protein that directly interacts with the shank family of proteins. *Mol. Cell. Neurosci.* 17, 385–397.
- Logan, S., et al., 2018. Simultaneous assessment of cognitive function, circadian rhythm, and spontaneous activity in aging mice. *Geroscience.* 40, 123–137.
- Logan, S., et al., 2019. Accelerated decline in cognition in a mouse model of increased oxidative stress. *Geroscience.* 41, 591–607.
- Luthi, A., et al., 1997. Endogenous serine protease inhibitor modulates epileptic activity and hippocampal long-term potentiation. *J. Neurosci.* 17, 4688–4699.
- Ma, H., et al., 2018. alpha2delta-1 couples to NMDA receptors in the hypothalamus to sustain sympathetic vasomotor activity in hypertension. *J. Physiol.* 596, 4269–4283.
- Macleod, G.T., Zinsmaier, K.E., 2006. Synaptic homeostasis on the fast track. *Neuron.* 52, 569–571.
- Maggio, N., et al., 2008. Thrombin induces long-term potentiation of reactivity to afferent stimulation and facilitates epileptic seizures in rat hippocampal slices: toward understanding the functional consequences of cerebrovascular insults. *J. Neurosci.* 28, 732–736.
- Makani, S., et al., 2012. NMDA receptor-dependent afterdepolarizations are curtailed by carbonic anhydrase 14: regulation of a short-term postsynaptic potentiation. *J. Neurosci.* 32, 16754–16762.
- Matsumoto-Miyai, K., et al., 2003. NMDA-dependent proteolysis of presynaptic adhesion molecule L1 in the hippocampus by neuropsin. *J. Neurosci.* 23, 7727–7736.
- Mattson, M.P., 2008. Glutamate and neurotrophic factors in neuronal plasticity and disease. *Ann. N. Y. Acad. Sci.* 1144, 97.
- Maurer, A.P., et al., 2017. Age-related changes in lateral entorhinal and CA3 neuron allocation predict poor performance on object discrimination. *Front. Syst. Neurosci.* 11, 49.
- Maxwell, C.R., et al., 2006. Ketamine produces lasting disruptions in encoding of sensory stimuli. *J. Pharmacol. Exp. Ther.* 316, 315–324.
- Mayer, M.L., et al., 1984. Voltage-dependent block by Mg²⁺ of NMDA responses in spinal cord neurones. *Nature.* 309, 261–263.
- Mayeux, J., et al., 2017. Inhibition of endocannabinoid degradation improves outcomes from mild traumatic brain injury: a mechanistic role for synaptic hyperexcitability. *J. Neurotrauma* 34, 436–443.
- Mayford, M., et al., 2012. Synapses and memory storage. *Cold Spring Harb. Perspect. Biol.* 4.
- McGuinness, L., et al., 2010. Presynaptic NMDARs in the hippocampus facilitate transmitter release at theta frequency. *Neuron.* 68, 1109–1127.
- McIntosh, A.R., 2000. Towards a network theory of cognition. *Neural Netw.* 13, 861–870.
- Meier, F., et al., 2020. diaPASEF: parallel accumulation-serial fragmentation combined with data-independent acquisition. *Nat. Methods* 17, 1229–1236.
- Monnerie, H., et al., 2010. Dendritic alterations after dynamic axonal stretch injury in vitro. *Exp. Neurol.* 224, 415–423.
- Muelbl, M.J., et al., 2018. Effects of mild blast traumatic brain injury on cognitive- and addiction-related behaviors. *Sci. Rep.* 8, 9941.
- Mukherjee, S., et al., 2020. Neuroinflammatory mechanisms of post-traumatic epilepsy. *J. Neuroinflammation* 17, 1–11.
- Nicole, O., et al., 2001. The proteolytic activity of tissue-plasminogen activator enhances NMDA receptor-mediated signaling. *Nat. Med.* 7, 59–64.
- Okada, K., et al., 2014. Enhanced flexibility of place discrimination learning by targeting striatal cholinergic interneurons. *Nat. Commun.* 5, 1–13.
- Olds, J.L., et al., 1990. Discrimination learning alters the distribution of protein kinase C in the hippocampus of rats. *J. Neurosci.* 10, 3707–3713.
- Ozen, L.J., Fernandes, M.A., 2012. Slowing down after a mild traumatic brain injury: a strategy to improve cognitive task performance? *Arch. Clin. Neuropsychol.* 27, 85–100.
- Panzer, M.B., et al., 2012a. A multiscale approach to blast Neurotrauma modeling: part I - development of novel test devices for in vivo and in vitro blast injury models. *Front. Neurol.* 3, 46.
- Panzer, M.B., et al., 2012b. Development of a finite element model for blast brain injury and the effects of CSF cavitation. *Ann. Biomed. Eng.* 40, 1530–1544.
- Park, K., Biederer, T., 2013. Neuronal adhesion and synapse organization in recovery after brain injury. *Future Neurol.* 8, 555–567.
- Pessoa, L., 2008. On the relationship between emotion and cognition. *Nat. Rev. Neurosci.* 9, 148–158.
- Prius-Mengual, J., et al., 2019. NMDA receptors containing GluN2B/2C/2D subunits mediate an increase in glutamate release at hippocampal CA3-CA1 synapses. *Mol. Neurobiol.* 56, 1694–1706.
- Przekwas, A., et al., 2016. Synaptic mechanisms of blast-induced brain injury. *Front. Neurol.* 7, 2.
- Rommelink, E., et al., 2016a. Cognitive flexibility deficits in a mouse model for the absence of full-length dystrophin. *Genes Brain Behav.* 15, 558–567.
- Rommelink, E., et al., 2016b. Measuring discrimination- and reversal learning in mouse models within 4 days and without prior food deprivation. *Learn. Mem.* 23, 660–667.
- Richter, S.H., 2020. Automated home-cage testing as a tool to improve reproducibility of behavioral research? *Front. Neurosci.* 14, 383.
- Rosenbaum, M.D., et al., 2009. Effects of cage-change frequency and bedding volume on mice and their microenvironment. *J. Am. Assoc. Lab. Anim. Sci.* 48, 763–773.
- Rubin, T.G., Lipton, M.L., 2019. Sex differences in animal models of traumatic brain injury. *J. Exp. Neurosci.* 13, 1179069519844020.
- Rubin, R.D., et al., 2014. The role of the hippocampus in flexible cognition and social behavior. *Front. Hum. Neurosci.* 8, 742.
- Rutter, B., et al., 2021. Shock wave physics as related to primary non-impact blast-induced traumatic brain injury. *Mil. Med.* 186, 601–609.
- Samson, A.L., et al., 2008. Tissue-type plasminogen activator requires a co-receptor to enhance NMDA receptor function. *J. Neurochem.* 107, 1091–1101.
- Savtchouk, I., et al., 2019. Circuit-specific control of the medial entorhinal inputs to the dentate gyrus by atypical presynaptic NMDARs activated by astrocytes. *Proc. Natl. Acad. Sci. U. S. A.* 116, 13602–13610.
- Shannon, P., et al., 2003. Cytoscape: a software environment for integrated models of biomolecular interaction networks. *Genome Res.* 13, 2498–2504.
- Simmons, M.M., et al., 2020. Neurological Effects of Repeated Exposure to Military Occupational Levels of Blast: A Review of Scientific Literature.
- Šišková, Z., et al., 2014. Dendritic structural degeneration is functionally linked to cellular hyperexcitability in a mouse model of Alzheimer's disease. *Neuron.* 84, 1023–1033.
- Song, H., et al., 2018a. Linking blast physics to biological outcomes in mild traumatic brain injury: narrative review and preliminary report of an open-field blast model. *Behav. Brain Res.* 340, 147–158.
- Song, H., et al., 2018b. Nanometer ultrastructural brain damage following low intensity primary blast wave exposure. *Neural Regen. Res.* 13, 1516–1519.
- Song, H., et al., 2018c. Ultrastructural brain abnormalities and associated behavioral changes in mice after low-intensity blast exposure. *Behav. Brain Res.* 347, 148–157.
- Song, H., et al., 2019. Proteomic analysis and biochemical correlates of mitochondrial dysfunction after low-intensity primary blast exposure. *J. Neurotrauma* 36, 1591–1605.
- Sosa, M.A.G., et al., 2017. Lack of chronic neuroinflammation in the absence of focal hemorrhage in a rat model of low-energy blast-induced TBI. *Acta Neuropathologica Communicat.* 5, 1–12.
- Stuhmiller, J.H., et al., 1991. The Physics and Mechanisms of Primary Blast Injury. Conventional Warfare: Ballistic, Blast, and Burn Injuries. Department of the Army, Office of the Surgeon General, pp. 241–270.
- Szklarczyk, D., et al., 2019. STRING v11: protein-protein association networks with increased coverage, supporting functional discovery in genome-wide experimental datasets. *Nucleic Acids Res.* 47, D607–D613.
- TBICoE, 2021. Total DoD TBI Worldwide Numbers, 2000-2021 Q2. <https://health.mil/Military-Health-Topics/Centers-of-Excellence/Traumatic-Brain-Injury-Center-of-Excellence/DOD-TBI-Worldwide-Numbers>.
- Teng, E., et al., 2000. Contrasting effects on discrimination learning after hippocampal and conjoint hippocampal-caudate lesions in monkeys. *J. Neurosci.* 20, 3853–3863.
- Voikar, V., Gaburro, S., 2020. Three pillars of automated home-cage Phenotyping of mice: novel findings, refinement, and reproducibility based on literature and experience. *Front. Behav. Neurosci.* 14, 575434.
- Wagner, A.K., et al., 2004. Evaluation of estrous cycle stage and gender on behavioral outcome after experimental traumatic brain injury. *Brain Res.* 998, 113–121.
- Wang, K.K., et al., 2018. An update on diagnostic and prognostic biomarkers for traumatic brain injury. *Expert. Rev. Mol. Diagn.* 18, 165–180.
- Weber, T., et al., 2019. The ankyrin repeat domain controls presynaptic localization of Drosophila Ankyrin2 and is essential for synaptic stability. *Front. Cell Develop. Biol.* 7, 148.
- Webster, K.M., et al., 2017. Inflammation in epileptogenesis after traumatic brain injury. *J. Neuroinflammation* 14, 1–17.
- White, E.R., et al., 2017. Mild traumatic brain injury produces long-lasting deficits in synaptic plasticity in the female juvenile Hippocampus. *J. Neurotrauma* 34, 1111–1123.
- Witkowski, E.D., et al., 2019. Rapid changes in synaptic strength after mild traumatic brain injury. *Front. Cell. Neurosci.* 13, 166.
- Yu, F., et al., 2020. Fast quantitative analysis of timsTOF PASEF data with MSFragger and IonQuant. *Mol. Cell. Proteomics* 19, 1575–1585.
- Yuan, H., et al., 2009. The serine protease plasmin cleaves the amino-terminal domain of the NR2A subunit to relieve zinc inhibition of the N-methyl-D-aspartate receptors. *J. Biol. Chem.* 284, 12862–12873.
- Zhou, J.J., et al., 2018. Enhanced hypothalamic NMDA receptor activity contributes to hyperactivity of HPA Axis in chronic stress in male rats. *Endocrinology.* 159, 1537–1546.